



**HAL**  
open science

## Characterization of microcracking of NCF composites under accelerated hygrothermal cycles: Influence of the stitching yarn and the style of biaxial NCF

A. Bezzou, Mael Péron, Pascal Casari, V. Singery, D. Ponsolle, Frédéric Jacquemin

### ► To cite this version:

A. Bezzou, Mael Péron, Pascal Casari, V. Singery, D. Ponsolle, et al.. Characterization of microcracking of NCF composites under accelerated hygrothermal cycles: Influence of the stitching yarn and the style of biaxial NCF. *Composites Part A: Applied Science and Manufacturing*, 2021, 149, pp.106507. 10.1016/j.compositesa.2021.106507 . hal-04056938

**HAL Id: hal-04056938**

**<https://hal.science/hal-04056938>**

Submitted on 3 Apr 2023

**HAL** is a multi-disciplinary open access archive for the deposit and dissemination of scientific research documents, whether they are published or not. The documents may come from teaching and research institutions in France or abroad, or from public or private research centers.

L'archive ouverte pluridisciplinaire **HAL**, est destinée au dépôt et à la diffusion de documents scientifiques de niveau recherche, publiés ou non, émanant des établissements d'enseignement et de recherche français ou étrangers, des laboratoires publics ou privés.



Distributed under a Creative Commons Attribution - NonCommercial - NoDerivatives 4.0 International License

# Characterization of microcracking of NCF composites under accelerated hygrothermal cycles: Influence of the stitching yarn and the style of biaxial NCF.

---

H. Bezzou<sup>a</sup>, M. Peron<sup>a\*</sup>, P. Casari<sup>a</sup>, V. Singery<sup>b</sup>, D. Ponsolle<sup>c</sup>, F. Jacquemin<sup>a</sup>

<sup>a</sup>Université de Nantes, Institut de Recherche en Génie Civil et Mécanique (GeM), 58 Rue Michel Ange, 44606 Saint Nazaire, France

<sup>b</sup>Chomarat, 39 Avenue de Chabannes, 07160 Le Cheylard, France

<sup>c</sup>Solvay Composite Materials, 501 W. 3<sup>rd</sup> St, Winona, MN55987, USA

\*Corresponding authors: [mael.peron@univ-nantes.fr](mailto:mael.peron@univ-nantes.fr) (Mael Peron)

---

## Abstract

In this paper, an analysis of the evolution of microcracking of Non-Crimp Fabric (NCF) polymer matrix laminates under hygrothermal loading is presented. These composites are reinforced with biaxial NCF styles ([+45/-45], [0/90], etc.) and manufactured by Liquid Resin Infusion (LRI). The samples are subjected to accelerated hygrothermal cycles that cause microcracks in specific resin-rich areas (RRA). Three types of microcracks were found to occur in the heterogeneous morphology of NCF. An experimental method based on 2D microscopic observations was adapted for the characterization of microcracking in several NCF laminates. 3D tomographic X-ray observations were performed to investigate the propagation and location of microcracks in the NCF volume. The influence of humidity on microcracking was investigated. The impact of several parameters on microcracking was discussed, in particular the stitching yarn size and styles of biaxial NCF used in laminates.

**Keywords:** Durability, Hygrothermal cycles, Microcracking, Non-Crimp Fabric Composites

---

## 1 Introduction

Subsonic aircrafts have an expected service life of 20,000 flight cycles in which the structures are subjected to high hygrothermal cycles [1]. Over long periods of time, these cycles might degrade polymer matrix composites (PMC), either by thermal degradations or by diffusion of moisture causing internal stresses high enough to produce cracks in multi-axial composites [2]. The thermal degradations can chemically or physically affect the properties of the polymer, and are highly dependent on the temperature range, which is defined by the transition temperature of the polymer [3]. Moisture induces the swelling of the matrix causing significant stress in a laminate with wet surface plies and dry core ones [4]. Moreover, composites consisting of fibers and matrix generally having different

coefficients of thermal expansion that are heated during manufacture may, on cooling, develop sufficiently high residual stresses causing cracks in the matrix [5,6]. Thermal loading can increase these internal stresses to values very close to the transverse strength of the laminate [7]. Indeed, in a laminate composite, the plies expand or contract in different directions depending on the stacking of the laminate. With an independent and stress-free ply, expansion or contraction occurs freely regardless of the orientation of the ply. But when the plies are turned in different orientations and laminated together, each ply will not be able to expand or contract according to its own coefficient of thermal expansion (CTE) due to the presence of adjacent plies. As the matrix has a lower in situ failure stress than the fiber, microcracks are created in the matrix. Microcracking can lead to profound changes in property, particularly in terms of CTE and rigidity [8,9]. Existing literature [8,10–13] shows that in a laminated composite, microcracks appear in the matrix, and they occur first in the vicinity of a defect (porosity, filaments, etc.). Generally, these microcracks are oriented through the thickness, parallel to each other and to the fibers and do not lead directly to the ruin of the laminate.

Over the past two decades, studies have been published on the quantitative prediction of thermal microcracking [2,14,15] and on the influence of hygrothermal ageing on the properties of composite materials [7,16–18], but few studies have focused on microcracking mechanisms under hygrothermal cycles. One of the first studies was carried out by Reynolds et al. [1] and focused on the degradation of a classic laminate PMC under different accelerated hygrothermal cycles. In this study, the authors have defined the so-called “Baseline” cycles in which each cycle lasts 160 min and includes two phases: a dry phase at 163°C and -54°C and another wet phase at 87°C and 85% relative humidity. In addition to the residual stresses due to thermal and chemical shrinkages, humidity can also induce internal (or hygroscopic) stresses that influence microcracking. In certain polymer matrix composites (e. g. epoxy, polyamide), hygrothermal ageing causes significant degradation of the matrix properties causing microcracks in the matrix due to residual stresses already present in the laminate [19,20]. However, few studies have been carried out on the distribution of moisture in polymer matrix composites [1,7,16,21,22]. Under the cyclic effect, the moisture profile can be varied near the surface but is always stable within the material [1,16]. Moreover, these moisture cycles do not cause microcracks in the interior but only on the surface of the specimens [1,7]. Furthermore, the effects of moisture on the fatigue behavior of polymer matrix composites have been shown to be important by Smith and Weitsman [23]. The authors examined the subject of wet fatigue on the polymer matrix composite ([0/90<sub>3</sub>]s) where they obtained fatigue results for both dry and saturated samples in water at 30°C. The authors attributed the fact that the saturated samples had reduced transverse cracking to relaxation of residual stresses induced after manufacture. Residual stress relaxation is caused by matrix swelling in the composite as a consequence of moisture absorption [7,21,24]. Nevertheless, caution should also be exercised when studying

hot/wet cycles on polymer matrix fibrous composites. Studies have shown that certain phenomena such as reversible plasticization of the matrix, decrease in glass transition temperature ( $T_g$ ) and degradation of the Matrix/Carbon fiber interfaces can occur under the influence of moisture at high temperatures [21,25,26].

Costa et al. [27] have exposed the PMC materials (T300/Bismaleimide) to 95% RH and 80°C for 9 weeks in a climatic chamber. The authors found that the moisture present in the laminate causes interfacial delamination leading to microcracking at the Resin/Carbon fiber interfaces.

In recent years, the advent of carbon fiber and low-cost manufacturing processes has led to new applications for composite materials in industrial sectors such as aeronautic and automotive. The traditional technique of producing complex parts where fiber layup is tightly controlled, is to use pre-impregnated unidirectional fiber tapes laid-up in a suitable stack on the mold tool and to cure the part in an autoclave [12]. This process has high manufacturing costs and is limited in the production of large parts. Due to their good drapability, the textile NCF are combined with manufacturing processes such as RFI (Resin Film Infusion) to produce complex and large composite structures while minimizing manufacturing costs compared to prepreg processes [28,29]. Indeed, NCF are textiles that consist of several differently oriented layers of unidirectional fibers that are stitched together with a thin yarn to obtain a fabric with structural integrity [30]. These reinforcements lead to a very attractive combination of high material characteristics and economical processing [12]. The absence of complex tow crimp in NCF can result in composites with a higher mechanical performance than woven fabrics [31]. However, despite the massive developments that have been achieved, the NCF of previous generations do not meet the specifications required by the aeronautical application regarding resistance to microcracking. The stitching yarn seems to be problematic, as it leads to the formation of resin-rich areas (RRA), thus causing multi-scale heterogeneities. Under the effect of hygrothermal cycling, these RRA are responsible for a large part of the microcracking of the NCF composite. The internal morphology of NCF composites is more heterogeneous than conventional laminates, and this morphology has a consensual influence on resistance to microcracking [10,30,32–34].

The morphology of RRA of NCF composites can depend on several parameters such as the type of yarn used (size and nature) and the ply stacking sequence [10,32,33]. The parameters used during the stitching process (pattern, stitch tension, stitch pitch, etc.) may also influence the RRA [12,30,35,36], even though this is not developed in the present study. Liotier et al. [10] have applied hygrothermal cycles which are composed of a preliminary phase of water absorption of 12 h at 50 °C and 95% RH followed by 400 pure thermal cycles with a duration of 1 hour for each cycle. The authors have studied three types of stitching yarns [10]: Polyester (PET) 76 dtex, Polyamide (PA) 76 dtex and Novoloid 30 Tex, which is larger. The authors found that PET yarns are the only yarns whose Resin/Yarn (Epoxy/PET) interfaces remain intact compared to the other yarns studied. In addition, PA yarn rarely

causes microcracking in the loops of the stitching yarn, even after 2000 cycles. Overall, it has been shown that microcracking can be delayed by using fine stitching yarns because they cause less RRA and a good holding of the Resin/Yarn interfaces. The study by Nguyen [32] shows that thicker stitching yarn such as PET 76 dtex causes significantly more RRA not only at the stitching holes but also at the inter-ply interface.

Furthermore, it was shown in study of Liotier et al. [10] that after 2000 hygrothermal cycles, the NCF [-45/+45]<sub>2S</sub> NCF sample has a total microcrack density of almost 2.5 cm<sup>-1</sup> per ply, while the [90/0]<sub>2S</sub> NCF sample has a value of 3.5 cm<sup>-1</sup>. The authors explain that this difference is justified by the difference in the orientation of the stitching line relative to the carbon fibers. For the same reason, it was observed in the study of Nguyen [32] that [90/0/90] biaxial plies are very disturbed compared to [-45/0/45] plies because of the larger RRA in the 90° plies.

As mentioned above, several parameters can influence the morphology and degree of complexity of RRA. It is therefore necessary to evaluate these parameters, in particular the effects of stitching yarns and the stacking of biaxial NCF style on the hygrothermal performance and the development of microcracking of NCF composites. This trend has opened up new challenges for the development of a new generation of multi-axial carbon fiber-based NCF reinforcements. Firstly, this study focuses on the effects of the size and nature of the stitching yarn on RRA. Secondly, the impact of the stacking of NCF styles will be studied (in present study, a NCF style is composed of two layers). Actually, two options for the manufacture of quasi-isotropic laminates will be proposed: a first option including the [0/90] styles and a second option without the [0/90] styles (i.e. only [+45/-45] styles are used in this option). The aim is to compare the two options in order to conclude on the effect of the NCF styles on RRA and microcracking. Finally, moisture saturation can be seen as a beneficial quantity to relieve pre-existing internal stresses in polymer matrix NCF laminates, including stresses due to manufacturing and hygrothermal loading. Given the highly heterogeneous morphology and RRA in NCF laminates, the effects of moisture on microcracking will also be investigated in this study.

## **2 Process and materials**

### **2.1 NCF manufacturing processes**

The production of NCF reinforcement mats is carried out using a new multi-axial “Cut & Lay” technology by Karl Mayer [37]. This operation ensures the alignment and flatness of the fibers without twisting. These fibers are deposited by robotic arms according to predefined orientations. They are then transformed into biaxial NCF ([0/90], [+45/-45], etc.) and stitched with a specifically chosen stitching yarn (Figure 1). When selecting a stitching yarn, it is important to choose a thin yarn (with linear density of few Tex) while taking into account that the yarn

will have to pass through the needle eye several times. In most cases, polyester and polyamide are the two types of yarn that can meet this selection [12]. There exist various stitch types in stitching patterns to join the layers of free fiber layers together (tricot, chain, tricot-chain, etc.) [37]. The stitching process has several parameters that can influence the morphology and properties of the resulting NCF styles. Figure 1 shows an example of a biaxial NCF [+45/-45] style that is stitched into a “tricot” pattern. Parameters A and B represent the stitch spacing between the stitches which are called the gauge (A) and the length (B) respectively.

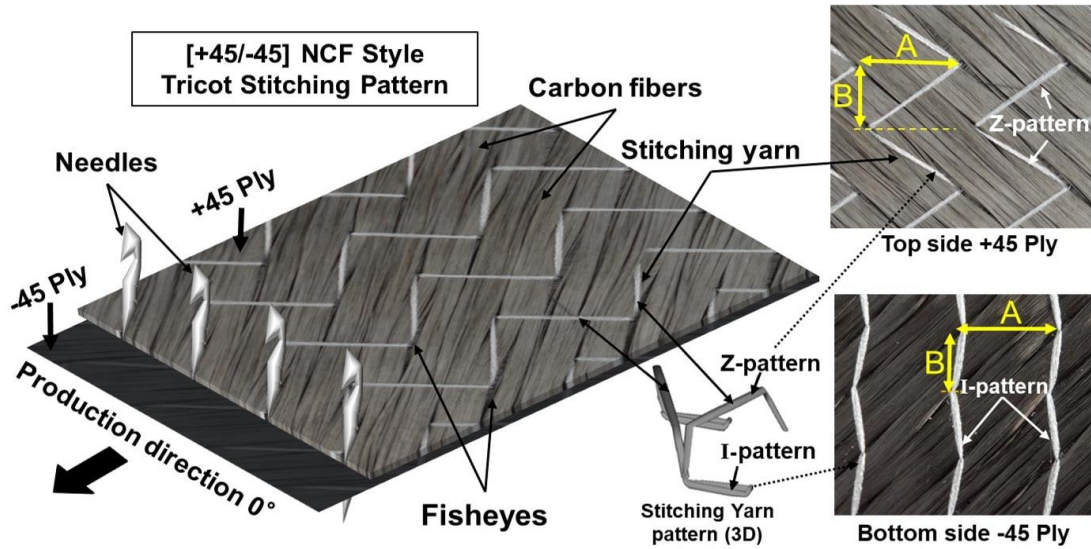


Figure 1. Schematic assembly of a reinforcement NCF [+45/-45] style stitched in “tricot” pattern.

## 2.2 Materials

The NCF laminate plates studied are quasi-isotropic layup  $[45/-45/0/90]_{2s}$  (QI) of 16 plies ( $450 \times 400 \times h$  mm<sup>3</sup>) and are manufactured with a biaxial NCF called C-PLY™ (provided by Chomarat). The matrix used is a reinforced epoxy resin called PRISM EP2400 (supplied by Solvay). The fibers used for biaxial NCF are made of carbon 24K IMS65. To manufacture NCF laminate plates for sample preparation (see sub-section 4.1 for sample preparation), biaxial NCF were impregnated with resin EP2400 using a vacuum-assisted resin infusion process and cured according to the instructions of the supplier. The EP2400 resin is first heated to 100°C in a vacuum oven and then vacuum degassed for 15 min. The infusion is made at 100°C under a vacuum of about 8 mbar, then the plate is heated at 2°C/min up to 180°C and held at 180°C for 2 hours and then cooled at 5°C/min down to 40°C, according to the Manufacturer’s Recommended Cure Cycle (MRCC). The target volume content of carbon fibers  $V_f$  is 57%. Once the plates have been manufactured, the values of the volume content  $V_f$  are calculated by two methods, either by measuring the thickness of the plate (knowing the weight and density of the carbon fibers) or by the ratio of the volumes of the components. Two options are chosen for the manufacture of laminates:

- **“Option A”**: the laminate QI layup  $[+45/-45/0/90]_{2s}$  is made by using 3 biaxial NCF styles: [+45/- 45],

[-45/+45] and [0/90] which are directly superposed without any necessary prior orientation. As a consequence, the stitching systems between the NCF styles are oriented parallel to each other, as illustrated in Figure 2-a.

- **“Option B”**: the laminate QI layup [+45/-45/0/90]<sub>2S</sub> is made by using a single style of biaxial NCF [+45/-45]. In order to ensure the (0°/90°) orientation in the laminate, biaxial NCF [+45/-45] styles are oriented -45° from the 0° direction, as shown in Figure 2-b. In this case, the orientation of stitching systems between the NCF styles is crossed (-45/0 or 0/-45).

It should be noted that the final stacking of the laminate is [+45/-45/0/90]<sub>2S</sub> (QI) and remains unchanged throughout this present study, regardless of the manufacturing option chosen.

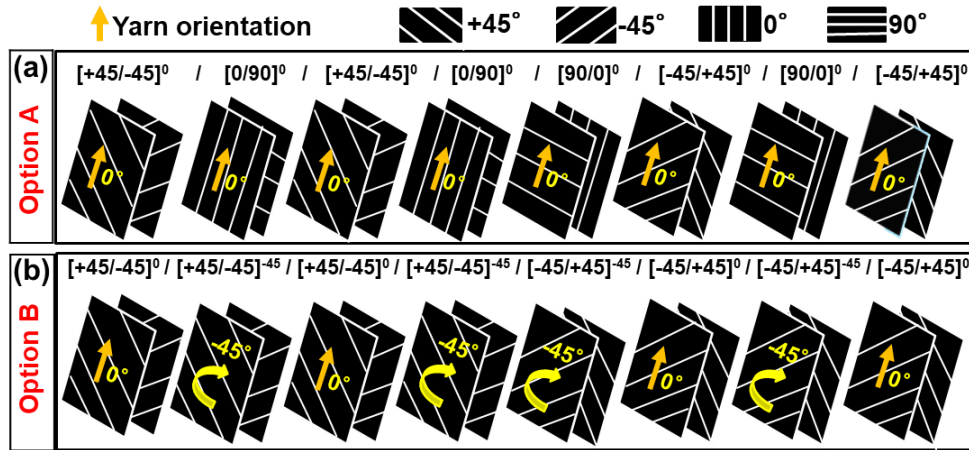


Figure 2. Schematization of the options chosen for manufacturing NCF [+45/-45/0/90]<sub>2S</sub> laminates. (a) “Option A” and (b) “Option B”.

Furthermore, two different types of stitching yarns are chosen for experimental characterization: Polyester (PET) 36 dtex (composed of 24 filaments) and Polyamide (PA) 39 dtex (composed of 34 filaments). The following Table 1 shows the configuration of the NCF laminates studied.

Table 1. Configuration of the NCF laminates studied.

Materials	Manufacturing option	V <sub>f</sub> (%)	Thickness h (mm)	Yarn nature	Yarn size
PET36-A	A	57	3.10	Polyester	36 dtex
PET36-B	B	56	3.15	Polyester	36 dtex
PA39-A	A	55	3.23	Polyamide	39 dtex
PA39-B	B	58	3.06	Polyamide	39 dtex

### 3 Hygrothermal loading

The application of a representative load for the environmental conditions of the service requires accelerated laboratory tests, allowing the same degradation to be caused in less time. In this study, the NCF composite was loaded 2000 times with an accelerated hygrothermal load representative of the operating conditions of a subsonic jet during its life cycle (Figure 3). These cycles do not follow exactly the same conditions as the aircraft during the flight, but they have been defined by considering the main elements of the real environment [38]. In this loading, there are 5 blocks of 400 cycles and each block is composed of two different loading phases: a first stationary phase called “water absorption” where the samples are exposed to 95% RH for 12 hours at 50°C and a second dry thermal cycling phase. During this last phase, the samples are cycled 400 times alternatively between an isothermal step at -54°C and one at +80°C, with a temperature rate of 9°C/min between each isothermal steps. Each cycle lasts one hour, and this logically gives a duration of 15 min for each temperature rise/decrease and 15 min for each isothermal step at 80°C and -54°C. Finally, it takes a total of about 3 months to reach the 2000 cycles.

The hygrothermal cycles were carried out using an experimental device respecting the hygrothermal cycles shown in Figure 3. This device consists of two parts: a climatic chamber for the wet conditioning (85% RH at 50°C) and the positive temperature of 80°C, and a freezer for the negative temperature of -54°C. In order to ensure the cycle between these two pieces of equipment (climatic chamber and freezer), a sample holder guided by a pneumatic system is used to transfer the samples automatically from one part to the other while respecting the imposed temperature cycle. The proper functioning of this device has been verified by controlling the temperature using three thermocouples: in the climatic chamber, in the freezer and on the sample holder. The temperatures are measured in real time during the applied cycles and represent the temperatures of the environment of each part. The temperature measured in the chamber is  $79.8 \pm 0.5^\circ\text{C}$ . The temperature measured in the freezer is  $-53.9 \pm 2^\circ\text{C}$ . Finally, the average values measured indicate that the rates are  $10.23^\circ\text{C}/\text{min}$  during heating and  $11.14^\circ\text{C}/\text{min}$  during cooling. Reynolds et al. [1] have shown that increasing rates (heating and cooling) has a negligible effect on the overall response to hygrothermal cycles. The authors of this study have demonstrated by accelerated hygrothermal cycles that the increase in rate of  $5^\circ\text{C}/\text{min}$  had no influence on either the thermal response or the internal equilibrium moisture concentration. However, in the present study, the same conditions (including heating/cooling rates) were applied to all samples to allow proper comparison of microcracking results.

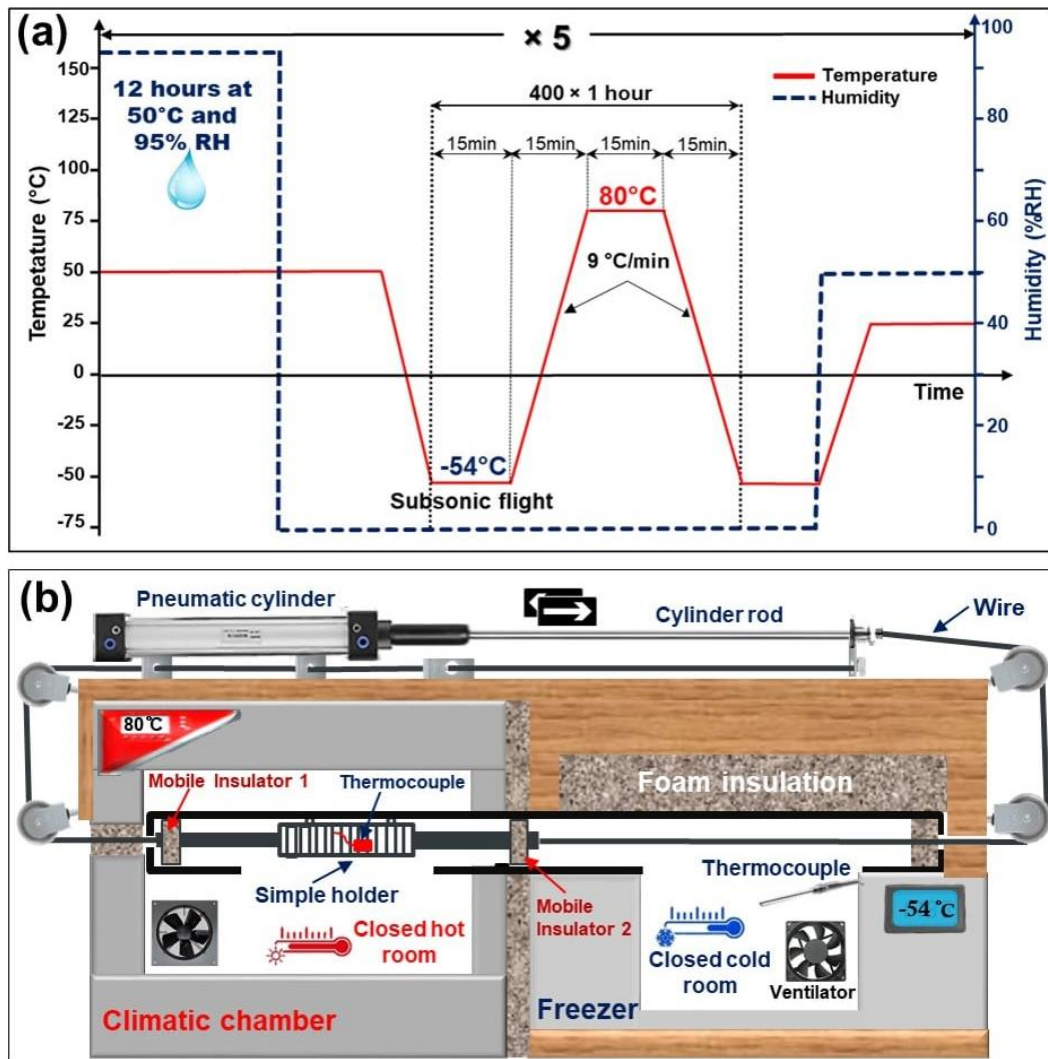


Figure 3. Applied hygrothermal loading cycles (a) and experimental device used (b).

In this present paper, in order to study the influence of relative humidity on the evolution of microcracking, loading cycles are applied on unconditioned samples (i.e. samples at ambient conditions) and on saturated samples at 85% RH and 70°C in a climatic chamber (EXCAL 5421) for about 192 days. The gravimetric method is carried out using a precision balance RADWAG (XA 82/220) with a resolution of  $10^{-5}$  mg, according to the standard “NF EN ISO 62”. The evolution of the average moisture content over time was investigated and it was found that the saturation point is reached on the studied samples after about 6 months of exposure to relative humidity. The saturation moisture content  $M_s$  (%) reached is 0.581 and 0,596 for PET36 and PA39 samples respectively.

## 4 Methods and analysis

### 4.1 Sample preparation

Hygrothermal cycles, as applied in this study, induce gradients of water concentration and stress profiles in regions close to the surfaces [8], [16]. Such cycles behave like hygrothermal fatigue on the material and can create microcracks in the laminate and more intensely near edges and exposed surfaces [40]. Composite materials are subjected to variable moisture concentration gradients during their service, thus producing internal hygrothermal stresses which can cause degradation of properties in the material [39]. Analysis of edge microcracking under accelerated hygrothermal cycles is complex due to thermal aging and water concentration gradients that cause variable stress concentration profiles near the edges [40]. For this reason, a cutting plan was specially chosen to ensure that the hygrothermal stresses caused by the load are similar throughout the samples analyzed. A depth of 5 mm affected by the water concentration gradient induced by hygrothermal loading (cf. Figure 3) has been estimated by Liotier et al. [10]. A 10 mm margin was added to the estimated length of 5 mm to ensure that the study area is homogeneous for microcracking analysis. On the other hand, previous studies on microcracking of NCF composites [32,33] showed that an observation section with 3 fisheyes in each ply is largely sufficient to be representative for microcracking analysis. For the C-PLY™ NCF studied in this paper it was estimated, by experimental measurements using an optical microscope, that “the gauge  $A$ ” between the fisheyes (cf. Figure 1) is equal to  $5.1 \pm 0.1$  mm. A sample length of 20 mm is chosen for the cut samples since it includes an observation length  $L$  containing at least 3 fisheyes. This means that the observation length  $L$  must be at least 3 times longer than the gauge  $A$  ( $L > 3 \times A$ ). Taking into account all the estimates mentioned in this paragraph, the minimum dimension of the representative samples to be subjected to hygrothermal cycles is  $50 \times 50 \times h$  mm<sup>3</sup>.

After each 400 hygrothermal cycles (12h of wet conditioning followed by 400 thermal cycles), the microcracking analysis samples with a size of  $20 \times 20 \times h$  mm<sup>3</sup> ( $h$  is the laminate thickness, see Table 1) are extracted from the center of the cycled samples according to the schematic section plan shown in **Erreur ! Source du renvoi introuvable.** The samples are cut at 0° to the direction of manufacture. These samples for analysis are carefully cut with a micro-slitter to avoid causing damage by cutting. The observations sections were polished with an Automatic Polisher (Struers TegraPol) by following the steps described in

. These steps allow to obtain a mirror polishing to eliminate any scratches that may cause uncertainties in the microcracking results. Microscopic observations were performed on all samples prior to cycling and no microcracks were detected. This shows that the manufacturing process and the preparation steps (cutting and

polishing) do not produce microcracks in the NCF studied. As the stitching length  $B$  between the fisheyes is about 3.3 mm (this value was estimated by statistical measurements using an optical microscope) three observation sections are specifically retained with a space of about 1.65 mm (length of half a fisheye) between each section to take into account the geometry of the fisheyes in the microcracking analysis (**Erreur ! Source du renvoi introuvable.**-b, c).

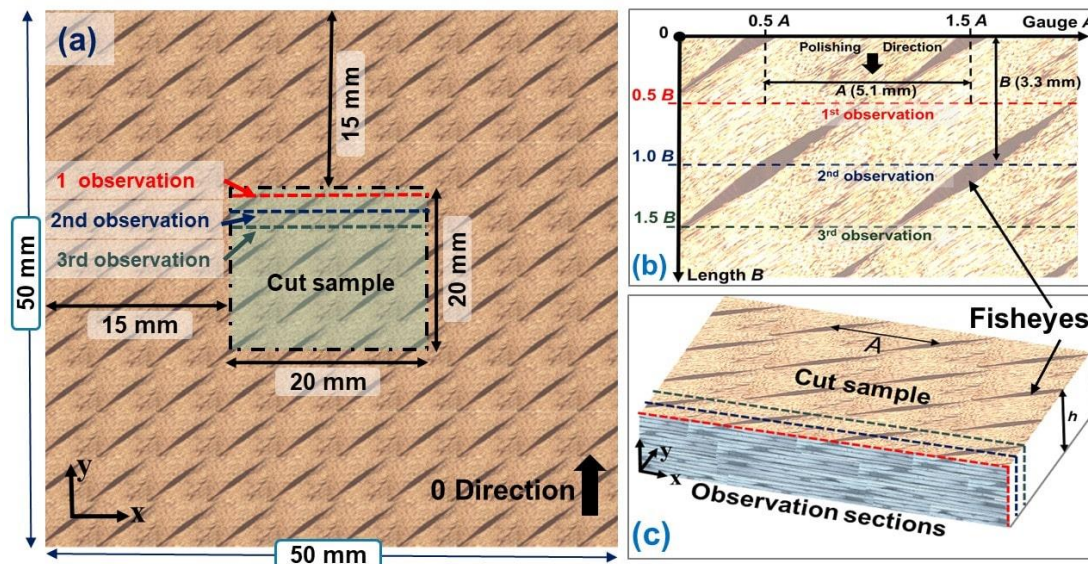


Figure 4. Cutting plan of the observations sections ( $20 \times 20 \text{ mm}^2$ ) for microcracking analysis.

Moreover, the samples are first cut with a low rotational speed ( $< 1000 \text{ rpm}$ ) and with a circular silicon carbide (SiC) milling cutter of a very thin thickness of 0.5 mm. Furthermore, after several polishing experiments, an optimal polishing protocol was successfully achieved for NCF composites reinforced with carbon fibers. The Figure 5 shows an example of a 2D micrograph of a sample of PET36-A which has been polished following the steps described in the **Erreur ! Source du renvoi introuvable.**. The microstructure of all samples (saturated or not in humidity) was observed before they were subjected to hydrothermal cycles. Observations were made with an optical microscope at the stitching filaments scale as shown in Figure 7-c. The observations show no porosities or microcracks due to manufacturing or preparation on the samples studied in this paper. The fact that no microcracks were observed on the unaged samples (zero cycle) allowed us to confirm the preparation protocol (cutting and polishing), and to assume that the microcracks that would be observed on the material of this experiment are from aging cycles and not from the preparation steps. Finally, for the microcracking analyses over the hydrothermal cycles, each  $N$  cycles ( $N=400$ ) requires the mentioned preparations on a single aged sample (one cut and three polishings as illustrated in **Erreur ! Source du renvoi introuvable.**). Thus, a complete analysis of 2000 cycles is performed on 5 different  $50 \times 50 \times h \text{ mm}^3$  samples for each kind of laminate (one sample for each  $N$

cycles). As the preparation protocol requires adapted to prevent variations due to edge effects, the samples analyzed at N cycles are not the same as those analyzed at N+400 cycles.

Table 2. Polishing protocol on an automatic polisher adapted to carbon fiber composite materials.  $V_1$  is the speed (rpm) of the principle platen (abrasive paper fixer) and  $V_2$  is the speed of the secondary platen (Sample Holder) of the automatic polishing machine.

Step	Abrasive paper	Grain size	Pression (N/cm <sup>2</sup> )	Time (min)	$V_1 / V_2$ (rpm)
1	P320	46 $\mu$ m	2.5	1-2	160/120
2	P800	22 $\mu$ m	2.5	1	160/120
3	P1200	15 $\mu$ m	2.5	2	160/120
4	P2000	10 $\mu$ m	2.0	2	150/100
5	P4000	5 $\mu$ m	2.0	4	150/100
6	4 min in the ultrasonic water bath				
7	MD-DAC	3 $\mu$ m	2.0	5	120/80
8	MD-NAP	1 $\mu$ m	2.0	4	120/80

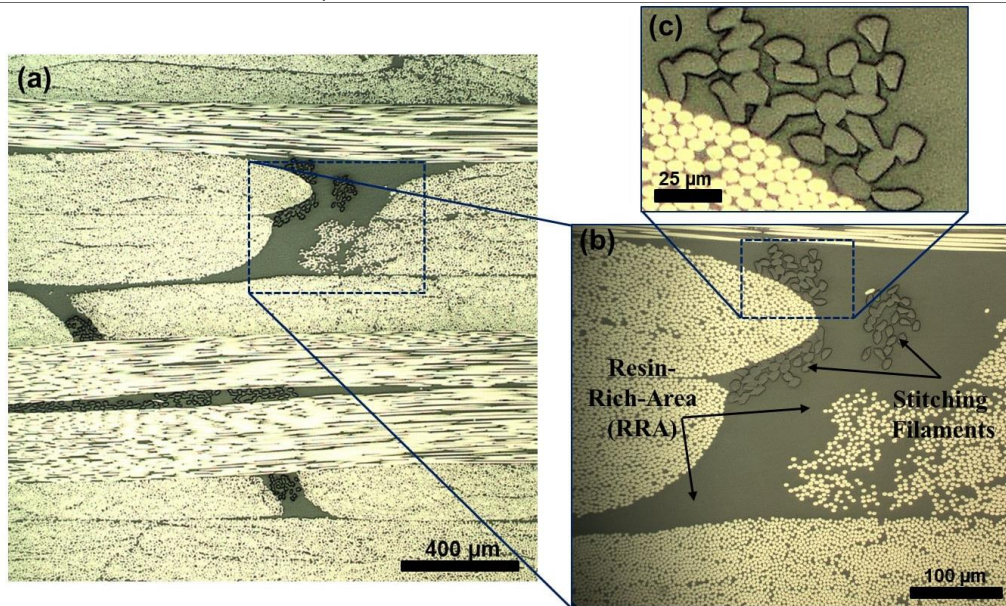


Figure 5. (a) 2D Observation of PET36-A under an optical microscope (b) RRA influenced by the PET yarn.

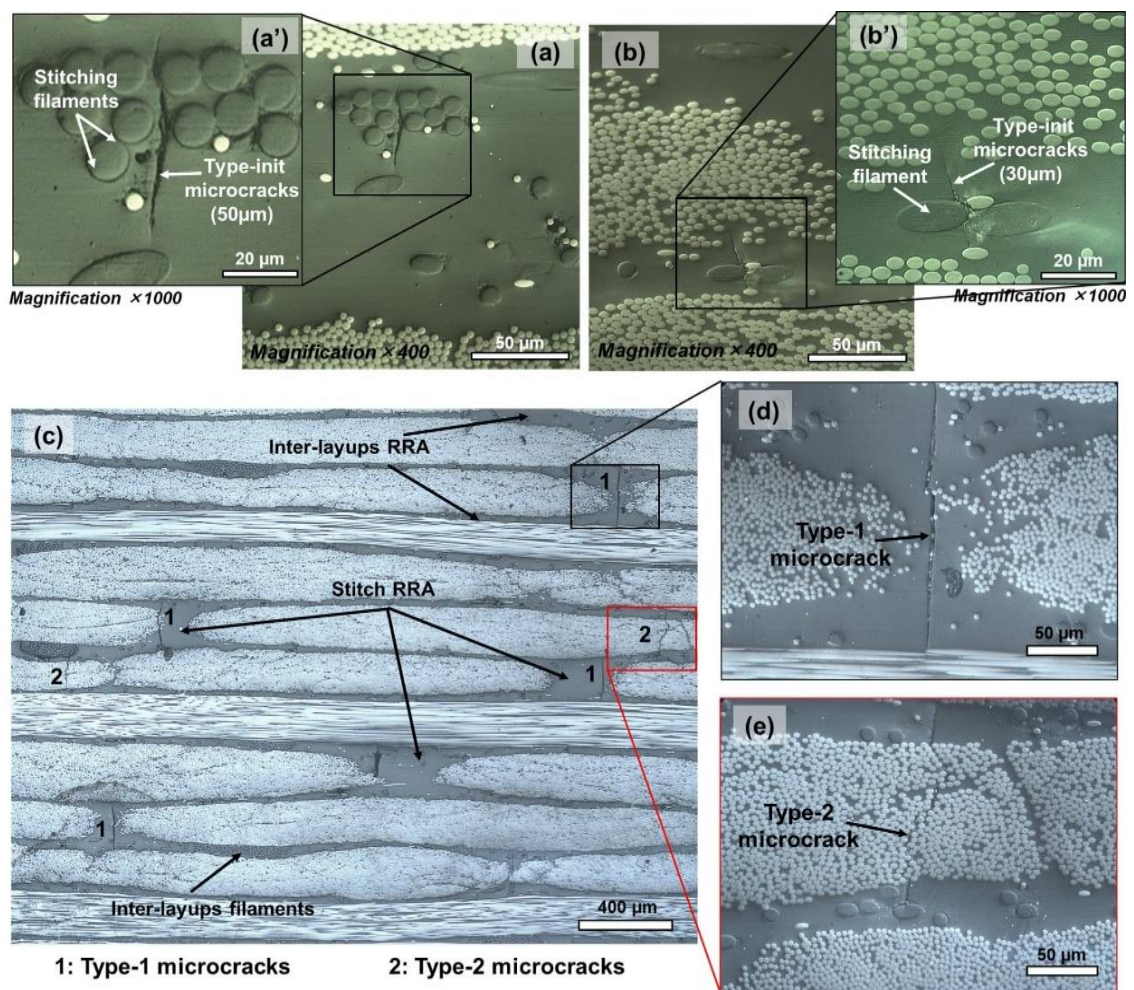
## 4.2 Types of microcracks in NCF composites

In NCF laminates, the difference between the properties of the resin, stitching filaments, and carbon fibers causes microcracks to occur at different locations in NCF subjected to hygrothermal cycling. In fact, microcracks in NCF laminates can occur at three different locations: near the sewing filaments, in the RRA of the stitches, and in the fibrous regions. These three types of microcracks are presented below in the order of occurrence in NCF laminates.

### 4.2.1 Type-init Microcracks

Due to the heterogeneous morphology of NCF laminates, microcracks may appear in different locations within the NCF composite. In addition, due to the difference between the properties of the resin and the stitching filaments,

the first microcracks, called "Type-init", were initiated at the Resin/Stitching filament interfaces and at the first hydrothermal cycles. These "Type-init" microcracks are small ( $<40\ \mu\text{m}$  at 400 cycles) and therefore require a rather large magnification under the optical microscope ranging from  $\times 400$  to  $\times 1000$  to be observed and measured correctly. Due to the stitching pattern of NCF, filaments may be present in both the stitch RRA (or in stitching loops where the stitching filaments cross the NCF) and in the RRA inter-layups (between the biaxial NCF layups). Therefore, the location of Type-init microcracks in the RRA depends on this feature, i.e., microcracks can be observed at the interfaces and near the filaments in the stitches (Figure 6-a, a') or in the RRA between the NCF layups (Figure 6-b, b').



- Figure 6. Observation and location of each type of microcrack in NCF laminate. Type-init microcracks in the Resin/Stitching filaments of the stitch RRA (a and a'). Microcracks in the Resin/Stitching filaments of the inter-layups (b and b'). "Type-1" and "Type-2" transverse microcracks (c) observed in the fisheye RRA (d) and in fibrous areas (e), respectively.

#### 4.2.2 Type-1 and Type-2 transverse microcracks

In addition, in NCF composites subjected to severe hydrothermal cycling ( $>800$  cycles), other types of microcracks are observed and have longer lengths than the Type-init microcracks presented above. As shown in Figure 6-c,

these other types of microcracks are transverse and cross at least the ply thickness ( $0,196 \pm 0,01$  mm) with the same direction as the ply in which they are located. These transverse microcracks can be classified into two types:

- **Type-1 microcracks:** these microcracks appear in the RRA of the fisheyes as shown in Figure 6-d. These microcracks are extremely dependent on the size of the stitch RRA of the fisheyes (i.e. size of stitching yarn) and generally appear after 800 hygrothermal cycles.
- **Type-2 microcracks:** these microcracks are common to all conventional composites and are detected in the fibrous areas (Resin/Carbon fibers) as shown in Figure 6-e. These microcracks are parallel to the carbon fibers and generally appear after the Type-1 transverse microcracks, i.e. after about 1200 cycles.

### 4.3 Adequate microcrack density

A complete characterization of the evolution of a variable representing the microcracking of a conventional UD composite subjected to a hygrothermal loading is presented in the study by Reynolds et al. [1]. The authors compare microcracking influenced by several types of hygrothermal cycles through a special variable, based on 2D microscopic observations, which they call “crack density”. Three years earlier, Maddocs [8] had also used the crack density variable in its study on microcracking in composites laminates under thermal and mechanical loading. It was shown that under cold thermal loading (from room temperature to  $-184^{\circ}\text{C}$ ), the first microcracks are visible between the plies [60/-60]. These microcracks are less than half the thickness of the ply and are not counted in the microcrack density measurements. For NCF composites, certain conditions must be taken into account when using this analysis method. Reynolds et al. [1] have defined a crack density variable to characterize a classic laminate PMC cracked under several types of hygrothermal cycles. In this study, the authors of this study have finally distinguished the cracks into four families according to the number of plies they traverse: “Single”, “Double” and “Triple” cracks traverse one, two and three plies of the group, respectively (referred as “ $N_1$ ”, “ $N_2$ ”, “ $N_3$ ” respectively). “Group” crack is defined as a crack that traverses the entire four ply group (referred as “ $N_4$ ”). To quantify the total density in a sample, the crack density variable can be written as follows:

$$\text{Crack density (cm}^{-1}\text{)} = \frac{(N_1) + (2N_2) + (3N_3) + (4N_4)}{SnL} \quad (\text{Eq.1})$$

Where “ $S$ ” is the number of samples analyzed, “ $n$ ” is the number of sides observed for each sample and “ $L$ ” is the observation length (in cm). The author applied this method to samples subjected to the hygrothermal cycles referred as “Baseline” (see introduction, paragraph 2) and found that these cycles cause a slow but regular increase in crack group density up to 500 cycles. Afterwards, the density values increase more rapidly until they reach the

stabilization stage after 1000 cycles, where they reach about 5 cm<sup>-1</sup>. The author notes that there is significant dispersion in all density data, especially at 1500 cycles, although no explanation was given for the causes of this dispersion. On the other hand, the variable developed by Reynolds et al. [1] aims to characterize the cracking in a plane perpendicular to the fibers of each ply, but this variable can only be used in unidirectional composites, because it does not take into account the orientation of the plies, such as 45° oriented plies. Generally, microcracks appear in the matrix and are oriented parallel to the fibers [9,40,41,10,42]. In order to quantify microcracks on multiaxial composites, Nguyen [32] added the parameter “sin (θ)” to the crack density variable to evaluate microcracks by taking into account the inclination of the fibers of each ply in NCF laminate. In this present study, in order to be able to make an independent analysis for each type of microcrack, another parameter was integrated into the microcrack density variable, namely parameter “d<sub>i</sub>”, with *i* = *init*, 1 and 2 for the *Type-init*, *Type-1*, *Type-2* microcracks, respectively. The final equation (Eq. 2) therefore takes into account both the type of microcracks (“*i*”) and the orientation of the fibers θ<sub>*j*</sub> of each ply “*j*”. The total microcrack density (d<sub>total</sub>) allows a global assessment of all quantified microcracks in the NCF laminate.

$$d_i = \frac{\sum_j \ell_{i,j} / t_j \sin \theta_j}{L.P} \quad \text{and} \quad d_{total} = \sum_i d_i \quad (\text{Eq.2})$$

Where “ℓ<sub>*i,j*</sub>” is the linear length of each type “*i*” of microcracks (*init*, 1 and 2) in the “*j*” ply of “*t<sub>j</sub>*” of thickness (0.196 ± 0.01 mm) and “θ<sub>*j*</sub>” orientation. *L* is the observation length, *P* is the number of plies considered, i.e. without the plies parallel to the observation plane. Since the gauge *A* is about 5.1 mm, the observation length chosen is 18 mm for all the samples analyzed, i.e. *L* contains at least three fisheyes in each ply (see the plan in **Erreur ! Source du renvoi introuvable.**-b). The *L* value of 18 mm is clearly longer than 3×*A* (≈15.3 mm). This variable of microcracks density (Eq.2) is based on micrographic observations under the optical microscope (Figure 7-b). Microcracks are measured in an observation plane of representative length *L* (Figure 7-c) on samples cut according to the cutting plane presented above (**Erreur ! Source du renvoi introuvable.**). The samples are then cycled from the ambient condition while respecting the hygrothermal cycles described in section 3 (Figure 3). A “Nikon Epiphot-TME” optical reflection microscope was used, coupled with the “Perfect Image software” for image acquisition and microcrack measurements. Before the observations and quantification of microcracks, the samples followed a specific preparation protocol ranging from cutting to polishing (sub-section 4.1). Microcrack quantification was performed each ply and at the scale of the fibers with a magnification objective ×400 whose resolution is 0.4 μm (as the resolution shown in the Figure 7-d). Subsequently, the microcracking data for each

type of microcrack (Type-init, Type-1 and Type-2) is determined in order to follow the evolution of the microcrack densities ( $\text{cm}^{-1}$ ) with the applied cycles using the formula defined by (Eq. 2). Indeed, to estimate the value of " $\ell_{i,j}$ " for each type of microcracks, it is required to analyze each ply " $j$ " considered in the laminate and for an observation length  $L$ . The linear length " $\ell_{init,j}$ " of Type-init microcracks is measured in each ply using the "Perfect-Image software" along the line of the observed microcrack with a magnification of  $\times 400$  as shown in Figure 7-d. Furthermore, the linear lengths " $\ell_{1,j}$ " and " $\ell_{2,j}$ ", which respectively correspond to Type-1 and Type-2 transverse microcracks, are assumed to be equivalent to the thickness of the ply " $j$ " in which they are observed. Therefore, Type-1 and Type-2 transverse microcracks are countable since their number  $N_{i,j}$  ( $i=1,2$  in this case) can be directly determined by the human eye in each ply " $j$ " of the NCF laminate analyzed. This means that the linear length " $\ell_{i,j}$ " of the transverse microcracks Type-1 or Type-2 in each ply is considered equal to the number  $N_{i,j}$  multiplied by the thickness " $t_j$ " of the ply ( $\ell_{i,j} = N_{i,j} \cdot t_j$ ). To evaluate the repeatability of the microcracking results, as shown in Figure 5, observations were performed on three observation sections in each sample subjected to a number of hygrothermal cycles. For the accuracy of the optical measurements (scales, lengths, etc.), a calibration was performed by using calibration standards specified for the different objectives lenses of the optical microscope used.

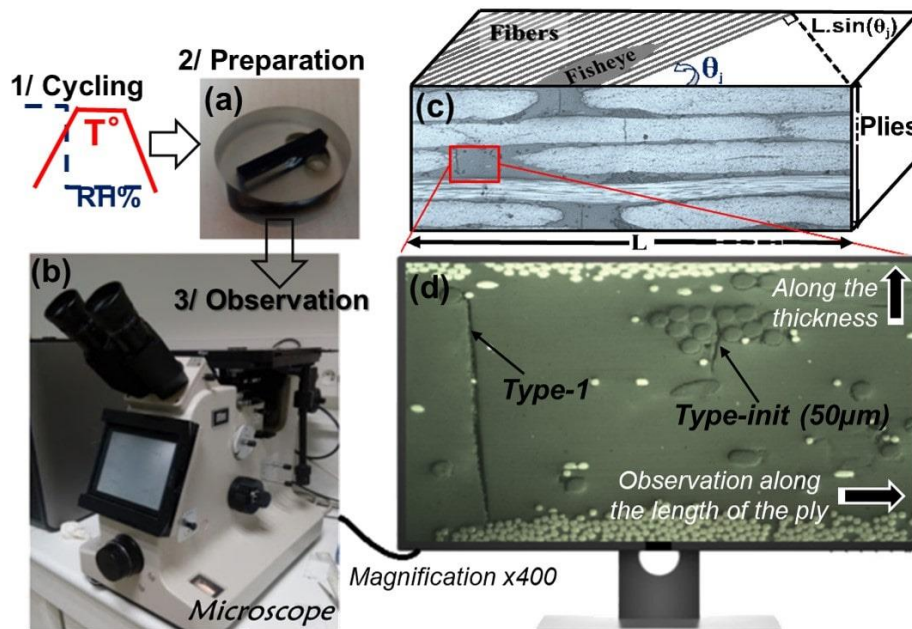


Figure 7. Different steps for quantifying microcracks.

## 5 Results and discussion

### 5.1 Influence of the stitching yarn on Resin-Rich Areas of fisheyes (RRA)

The stitching yarns cause the carbon fibers to deviate in a ply from their uniform direction. These deviations produce particulate forms so called “Fisheye” (Figure 1, Erreur ! Source du renvoi introuvable.) which become RRA after infusion impregnation (Figure 8). During the process of stitching biaxial NCF of different orientations, the fiber bundles can be placed in any orientation, it is not guaranteed that the knitting needles will pass through the plies precisely between these fiber bundles. The needles can penetrate the spread fiber bundles, and the production parameters of the machine (stitching speed, stitching pattern, etc.) are adjusted to minimize possible damage to the fibers (Such that the needles penetrate between the spread fiber bundles) [43]. This process results in a certain disturbance of the uniform placement of the fibers. Fisheyes are formed around the stitch holes due to the movement of the in-plane fibers. Figure 8 shows a 2D micrograph of an example of fisheye oriented at  $45^\circ$  before and after infusion impregnation. The parameters  $L_f$  and  $d_f$  represent the length and thickness of the fisheye, respectively (Figure 8). In this study, the fisheyes parameters  $L_f$  and  $d_f$  were estimated for each NCF studied in order to determine the influence of yarn type on the average size of the fisheyes in the NCF laminate. As mentioned above, RRA have a significant influence on the microcracking of NCF composites. It is therefore important to characterize the effects of different types of stitching yarns on the RRA of fisheyes.

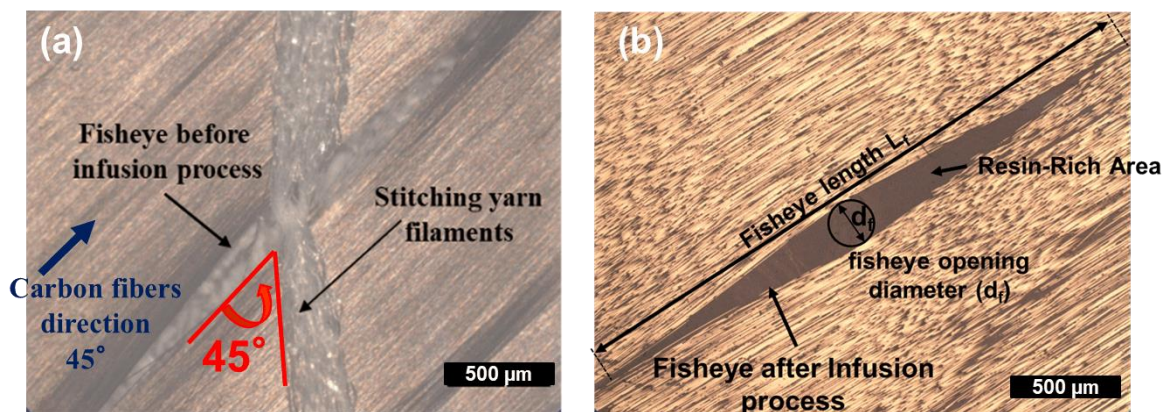


Figure 8. Fisheye oriented at  $-45^\circ$  before (a) and after (b) manufacture. The experimental measurements of  $L_f$  and  $d_f$  are carried out on NCF composites after their manufacture. The samples are polished in the  $XY$  plane, parallel to the plies (see Erreur ! Source du renvoi introuvable.) according to the polishing steps described in Erreur ! Source du renvoi introuvable.. For each sample, the volume abraded according to thickness is controlled during polishing so that the measurements of  $L_f$  and  $d_f$  are made on four plies oriented at:  $+45$ ,  $-45$ ,  $0$  and  $90^\circ$  ( $[+45/-45]$  and  $[0/90]$  NCF styles). These measurements were performed on ten different fisheye for each type of composite studied. The average values of the parameters  $L_f$  and  $d_f$  is presented

in Table 3. It can be seen that the length and opening of the fisheyes depends on the orientation of the plies of the laminate. Plies oriented at  $0^\circ$  have higher  $L_f$  and  $d_f$  values than other plies oriented at  $\pm 45^\circ$  and  $90^\circ$ . These results show that the length and opening of the fisheyes is greater in the NCF [0/90] styles than in the NCF [+45/-45] styles. It can also be noted that the fisheye lengths and openings are slightly longer in PA 39 dtex than in PET 36 dtex. It is clear that the size of the stitching yarn conditions the size of the fisheyes in NCF laminate.

Table 3. Estimation of fisheyes length  $L_f$  and opening  $d_f$ .

Stitching Yarn	Fisheyes length $L_f$ and opening $d_f$ (mm)				
	Parameters	+45°	-45°	0°	90°
PET 36 dtex	$L_f$	5.13±0.37	5.48±0.45	6.19±1.0	5.56±0.71
	$d_f$	0.18±0.05	0.23±0.09	0.28±0.12	0.25±0.05
PA 39 dtex	$L_f$	5.32±0.49	5.89±0.62	6.53±1.2	5.77±0.69
	$d_f$	0.23±0.07	0.28±0.11	0.34±0.14	0.30±0.08

These results of  $L_f$  and  $d_f$  show that the size of the yarn and the orientation of the carbon fiber ply influence the size of the fisheyes in the laminate. Therefore, “Option A” has a higher RRA in fisheyes since this option includes NCF [0/90] styles (see Figure 2). Considering that four of the NCF [0/90] styles are used for a 16-ply [+45/-45/0/90]<sub>2S</sub> laminate, the difference between “Option A” and “Option B” becomes more important and more obvious. Liotier et al, [33] characterized RRA influenced by fisheyes on two types of multiaxial NCF ([90/0]<sub>S</sub> and [+45/-45]<sub>S</sub>) stitched with yarn of Novoloid 30 tex. They measured  $L_f$  and  $d_f$  and found that the size of the fisheyes increases with the stacking sequence [0/90]. For example, they measured the  $d_f$  and found an average value of 0.47 mm for [+45/45] and 0.91 mm for [0/90]. This means that the opening of the fisheye is twice as large in [0/90]<sub>S</sub> as in [+45/-45]<sub>S</sub>. The authors have done the same measurements with other thinner yarns (PET and PA of 76 dtex) and conclude that the size of the fisheyes also depends on the type of yarn used. Basically, a thicker yarn produces larger fisheyes in the NCF.

## 5.2 Effects of stitching yarn and the style of NCF on microcracking

The interest here is to present separately the microcrack density for each type of microcrack to correlate each type of microcrack to the biaxial NCF styles stacking used. All the evolutions of microcrack densities are estimated using the approach detailed in sub-section 4.2. These evolutions are measured after each hygrothermal loading sequence: 400, 800, 1200, 1600 and 2000 cycles. As a reminder, the stacking of the studied NCF laminates is

[+45/-45/0/90]<sub>2S</sub>. As previously mentioned, the stacking of the laminates does not change, the study focuses on the orientation of the biaxial NCF styles (dry fabrics) used to manufacture these laminates of 16 plies:

- **NCF “option A” laminates:** use of 3 biaxial NCF styles: [+45/-45]×2, [-45/+45]×2, [0/90]×4.
- **NCF “option B” laminates:** use of one biaxial NCF styles: [+45/-45]×8.

Figure 9-a shows the evolution of the density of Type-init microcracks ( $d_{init}$ ) with hygrothermal cycles applied. As shown in this figure, Type-init microcracks seem to appear as soon as the first 400 hygrothermal cycles are applied. At 400 cycles, the PA39 sample reaches a Type-init density value of 0.33 cm<sup>-1</sup> for “option A” and 0.23 cm<sup>-1</sup> for “option B”, and all other laminates have a microcrack density of less than 0.15 cm<sup>-1</sup>. Then, the increase is progressive for all the materials up to 1200 cycles. Above this value, the evolutions for PA39 and PET39 samples begin to stabilize and the increase of these microcracks is reduced during the last hygrothermal cycles. At 2000 cycles, the PA39 sample has a density of 0.64 cm<sup>-1</sup> for “option A” and 0.52 cm<sup>-1</sup> for “option B”, while the PET36 laminates reach 0.48 cm<sup>-1</sup> for “option B” and 0.38 cm<sup>-1</sup> for “option B”. Furthermore, as shown by the results on microcrack density (Figure 9-a, b and c), no transverse microcracks Type-1 and Type-2 were detected at 400 cycles, whereas Type-init microcracks are already present. Type-init microcracks are smaller in size than the other transverse microcracks (Type-1 and Type-2), with dimensions between 0.04 mm and 0.12 mm (at 400 and 2000 cycles, respectively). As the number of cycles increases, the Type-init microcracks apparently develop in length, opening and also depth to become transverse microcrack. This could explain the small variation in these microcracks between 1200 and 2000 cycles. This evolution, which progresses weakly after 1200 cycles, indicates that other Type-init microcracks would have appeared to compensate for the eventual transition from Type-init microcracks to transverse microcracks.

Therefore, the comparison between “options A” and “option B” provides information on the influence of the size of the RRA which are smaller in the [+45/-45] styles than in the [0/90] styles (as shown in sub-section 5.1). Figure 9-b shows the evolution of the density of Type-1 transverse microcracks ( $d_I$ ) according to the applied hygrothermal cycles. These Type-1 microcracks appear and propagate along the RRA of the fisheyes. It can be seen in Figure 9-b that no microcracks Type-1 were found at 400 cycles for all laminates in this experiment. After 800 cycles, the evolution of the microcrack densities increases progressively with the cycles and they do not converge towards stabilization but evolve in a monotone way until 2000 cycles. At 2000 cycles, the PA39 samples achieve microcrack densities of 1.05 cm<sup>-1</sup> for “option A” and 0.64 cm<sup>-1</sup> for “option B”, while PET36 samples reach densities values of 0.7 cm<sup>-1</sup> for “option A” and 0.48 cm<sup>-1</sup> for “option B”.

Type-2 microcracks are also transverse, they are specific to conventional materials and are detected in Resin/Carbon fibers areas. These microcracks appear rather in the internal plies and they propagate along the carbon fibers. Figure 9-c shows the evolution of the density of these Type-2 microcracks ( $d_2$ ) with the applied hygrothermal cycles. It can be seen that these microcracks do not appear up to 1200 cycles for all the studied laminates. After 1200 cycles, a significant increase is obtained for the PA39 sample, reaching a microcrack density of  $0.34 \text{ cm}^{-1}$  for “option A” and  $0.25 \text{ cm}^{-1}$  for “option B” at 2000 cycles. A similar evolution is found for the PET36 sample, reaching values of  $0.28 \text{ cm}^{-1}$  for “option A” and  $0.20 \text{ cm}^{-1}$  for “option B” at 2000 cycles. These microcracks always appear after Type-1 microcracks, they are rather localized in the internal plies. This observation was already pronounced in the study of Nguyen [32]. This author showed by 3D tomographic observations that these Type-2 microcracks have limited lengths and propagate in the direction of the carbon fibers.

Figure 9-d shows the evolution of the total microcrack density ( $d_{total}$ ) with hygrothermal cycles applied. It can be seen that the evolution of the total microcrack densities is similar to the evolution of the density of Type-1 microcracks. Also, this figure allows us to compare all the microcracks measured for each type of samples studied and shows clearly that “option B” gives less microcracking than “option A”. Consequently, the evolution and quantity of microcracks depend on the stacking sequence of the NCF styles used in the manufacture of NCF laminates.

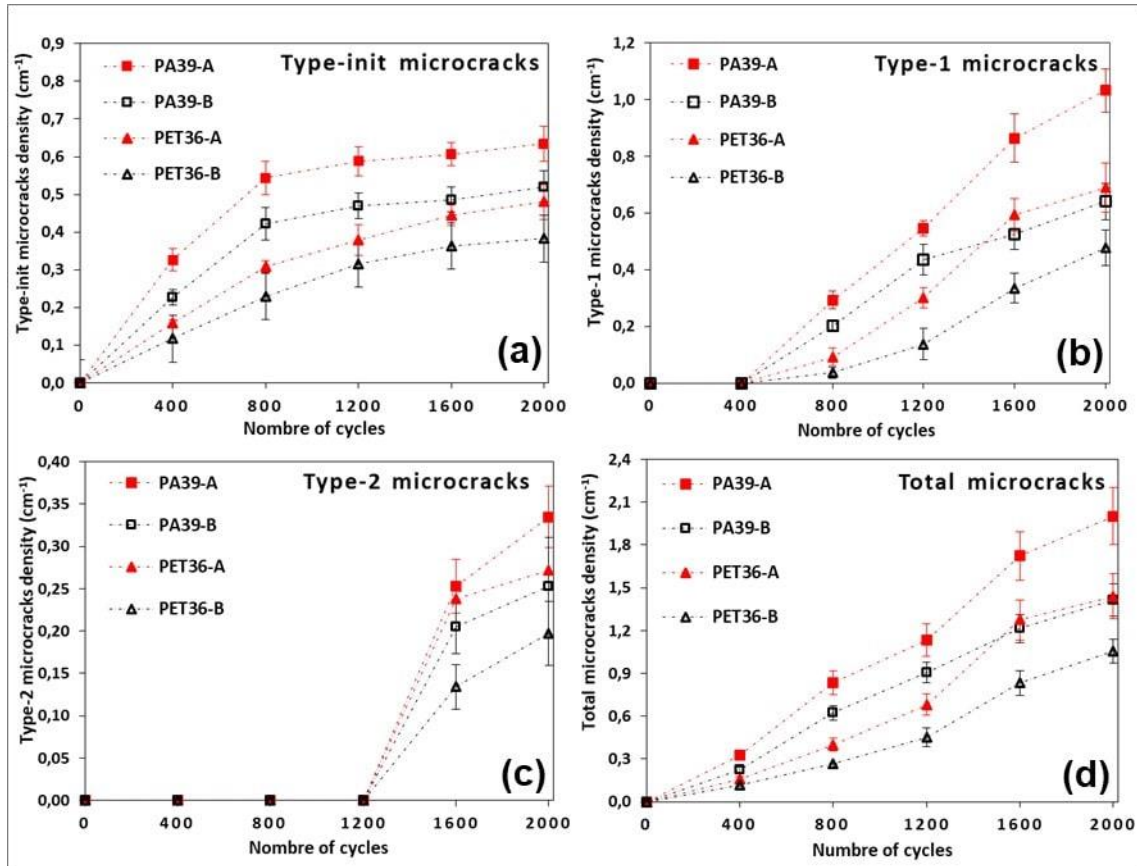


Figure 9. Comparison of Type-init (a), Type-1 (b), Type-2 (c) and total (d) microcracks under hygrothermal cycles between options A and B.

Figure 10 gives the percentage of total microcracks in the four biaxial NCF [0/90] and [+45/-45] styles used for PA39-A sample (i.e. the eight layers in the center of the sample), which is the most cracked sample. It is clear from this histogram that the difference in microcrack distribution between the two cases is significant. At 400 cycles, the biaxial NCF [0/90] styles cover 4 times more total microcracks than the biaxial NCF [45/-45] styles. This difference progressively reduces over the applied cycles, and at 2000 cycles the biaxial NCF [0/90] styles have 2 times more microcracks than the biaxial NCF [+45/-45] styles. Indeed, the difference in microcracking between these two options is necessarily due to the difference in RRA morphology between these two options. The results obtained in the section showed that the fisheyes are larger in “option A” than in “option B”. This could result in larger areas in “option A”. This difference in size and morphology probably leads to a different hygro-thermo-mechanical properties between the different constituents (resin, stitching yarn and carbon fibers), to which this difference in microcracking can be attributed.

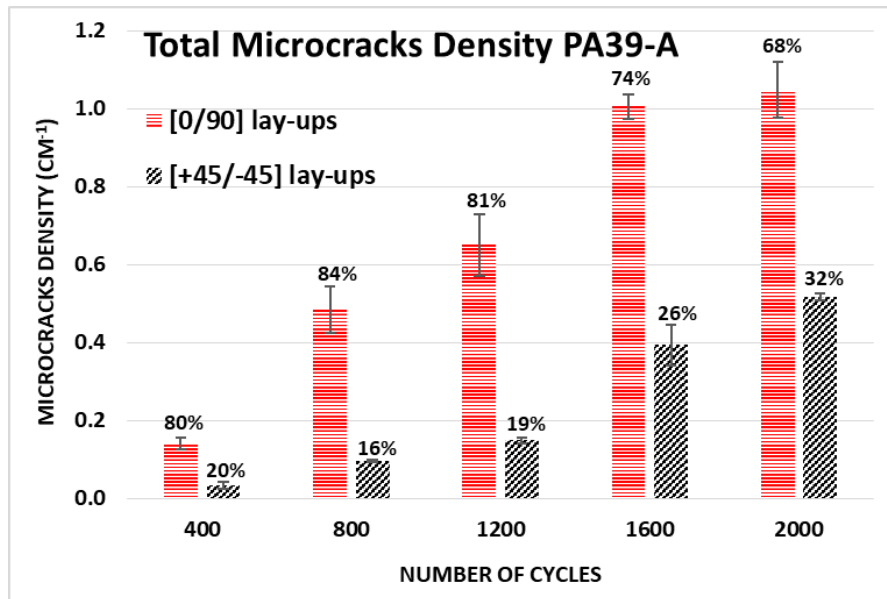


Figure 10. Histogram of total microcracks in the [0/90] and [+45/-45] NCF styles for PA39-A under hygrothermal cycles.

### 5.3 Effect of moisture saturation on microcracking

The effect of moisture on microcracking can be observed by comparing the results obtained on unsaturated samples (ambient conditions) and saturated samples (at 85% RH for about 6 months). **Erreur ! Source du renvoi introuvable.**-a shows the evolution of the density of Type-init microcracks (Resin/Stitching filaments microcracks) in saturated and unsaturated samples as a function of the cycles. The response of saturated samples to microcracking is slightly less severe than that of unsaturated samples referenced before 1000 cycles. Again, moisture seems to delay the appearance of the microcracks specifically at the Resin/Stitching filament interfaces. **Erreur ! Source du renvoi introuvable.**-b shows the densities of Type-1 microcracks (RRA of the fisheyes microcracks) obtained on unsaturated and saturated samples. As it can be seen that no Type-1 transverse microcracks were detected at 400 cycles. From 800 cycles, and for both PET36-A and PA39-A materials, the microcrack densities  $d_l$  of the saturated samples are uniformly lower than the microcrack densities  $d_l$  of the unsaturated samples. For PET36-A laminate, the difference is around 27% at 1200 cycles, 21% at 1600 cycles and 8% at 2000 cycles. For PA39-A laminate, the difference is about 31% at 1200 cycles, 23% at 1600 cycles and 10% at 2000 cycles. Moisture saturation results a decrease in the density  $d_l$  of the microcracks detected in the RRA at the stitches, although around 2000 cycles, the effect of moisture becomes comparatively less significant. Nguyen [32] has studied the effect of moisture by comparing pure thermal cycles and hygrothermal cycles with a period of prior saturation (30 days at 85% RH and 70°C). The author has applied these cycles to NCF composites and has concluded that moisture can have a beneficial role and decrease cracking densities during the first 1600 cycles. Nevertheless, according to the author, the behavior of the material seems to be modified after 1600 cycles due to

changes in physical and chemical properties of the resin epoxy. **Erreur ! Source du renvoi introuvable.**-c shows the evolution of Type-2 microcrack density (at “Resin/Carbon fibers” areas) for saturated and unsaturated samples. The average microcrack density response of saturated samples shows microcracking as early as 1200 cycles ( $d_2 = 0.11 \text{ cm}^{-1}$  for PA39-A\_SAT and  $d_2 = 0.56$  for PA39-A\_SAT), while unsaturated samples show no microcracks at this number of cycles. Unlike the Type-1 microcracks, the Type-2 microcracks observed at the “Resin/Carbon fibers” areas seem to be influenced and increased by the saturation of relative humidity (192 days at 85%RH and 70°C).

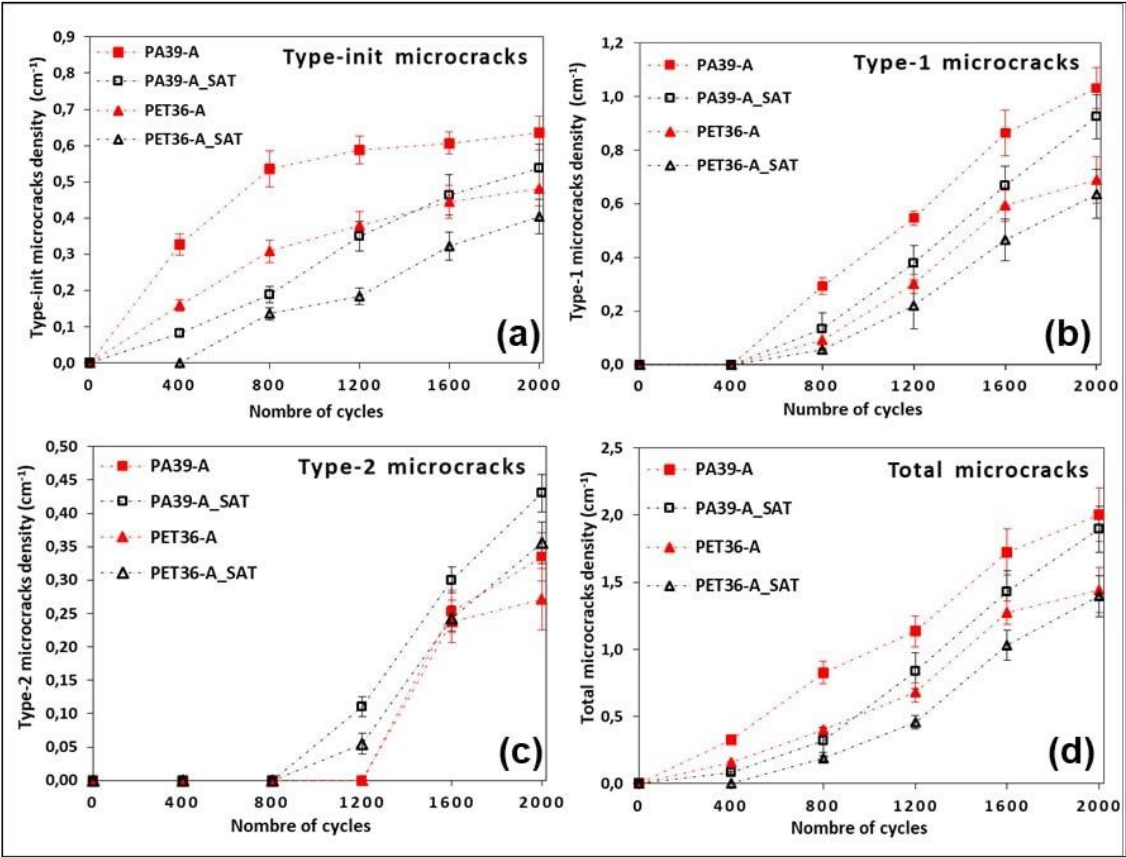


Figure 11. Comparison of Type-init (a), Type-1 (b), Type-2 (c) and total (d) microcracks density between unsaturated and saturated samples.

Total microcrack densities ( $d_{total}$ ) for saturated and unsaturated samples are presented in **Erreur ! Source du renvoi introuvable.**-d. This figure illustrates the difference in total microcrack evolution under hygrothermal cycles and shows that saturated samples cause less microcracking than unsaturated samples. For example, at 800 cycles, the density of microcracks in the PA39-A sample rapidly reaches a value of about  $d_{total} = 0.84 \text{ cm}^{-1}$ , while in the PA39-A\_SAT sample, the density value reached is about  $d_{total} = 0.32 \text{ cm}^{-1}$ . It appears that moisture saturation of the samples leads to a decrease/delay in the total microcrack density in NCF laminates. This may be related to the advantageous effect of moisture which limits the internal stress state due to hygrothermal processing and

loading. This can be related to the advantageous effect of humidity, which limits the internal stresses due to the processing and hygrothermal loads.

## **5.4 Effects of stitching and RRA on the propagation of microcracks**

### **5.4.1 SEM observation of first microcracks**

In order to characterize the first Type -init microcracks in the NCF, the Resin/Stitching filament interfaces can be observed with the scanning electron microscope (SEM). The samples are observed without micrometric film deposition and with a "Zeiss EVO 40" SEM. The SEM can be operated in vacuum (HV mode [ $10^4$ ;  $5 \cdot 10^{-3}$ ] Pa), in partial pressure (EP mode [10; 25] Pa) or in environmental conditions. The objective is to examine the state of the samples after manufacturing (without hygrothermal cycles) and to observe the Type-init microcracks at 400 hygrothermal cycles. The Resin/Stitching filament interfaces are inspected on unaged samples and on samples subjected to 400 hygrothermal cycles. It should be mentioned that it is sometimes difficult to detect the polyester filaments in the resin due to the low contrast between these two constituents, and especially if the magnification is very high. Moreover, when we increase the energy of the electrons (to obtain more interaction with the material and a better contrast between the constituents), the surface charge effects remain and can affect the imaging by giving wrong information during the analysis. Therefore, in order to observe details with the least amount of charge effect, we made a compromise by choosing a working distance (WD) of 4 mm and an acceleration voltage of 30 kV for the images observed in backscattered electron mode (this mode is less sensitive to charge effects).

SEM observations on the unaged PET36-A samples show that there are no microcracks or micro-delamination between the matrix and the filaments and/or carbon fibers, neither in the stitch RRA (Figure 12-a and a'), nor in the inter-layup RRA (Figure 12-b and b'). As already observed by the optical microscope, the SEM observations show that the sample preparation steps (cutting and polishing) do not cause microcracks/defects that could have an impact on the microcracking analyses of the aged samples by the hygrothermal cycles. Subsequently, SEM observations were performed on the same kind of the laminate (PET36-A) but this time subjected to 400 hygrothermal cycles. Figure 12-c shows the stitching filaments present in the transverse plane on the surface of the sample. A cross-section through the thickness of the sample (a section along the dotted line) shows the existence of Type-init microcracks in the RRA (Figure 12-c1). SEM measures indicate that the length of these microcracks is in the range of  $25\mu\text{m}$  to  $45\mu\text{m}$  for this sample stitched with the PET 36dtex and subjected to 400 cycles. Furthermore, it appears in Figure 12-c1' that Type-init microcracks are initiated at the Resin/Stitching filament interfaces and which then seem to propagate through the thickness of the ply. It also appeared that

Type-init microcracks take a different trajectory when they are located far or near the filaments: their trajectory is straight when they propagate unrestricted in the RRA (Figure 12-c1'), while their trajectory follows the filament lines when they are located near the Resin/Stitching filament interfaces (Figure 12-c2). This last statement is already observed in the work of Liotier et al. [33] where the authors showed by SEM observations that the Resin/Stitching filament interfaces (Epoxy/PET) were the privileged way for the propagation of the first microcracks under hygrothermal cycles.

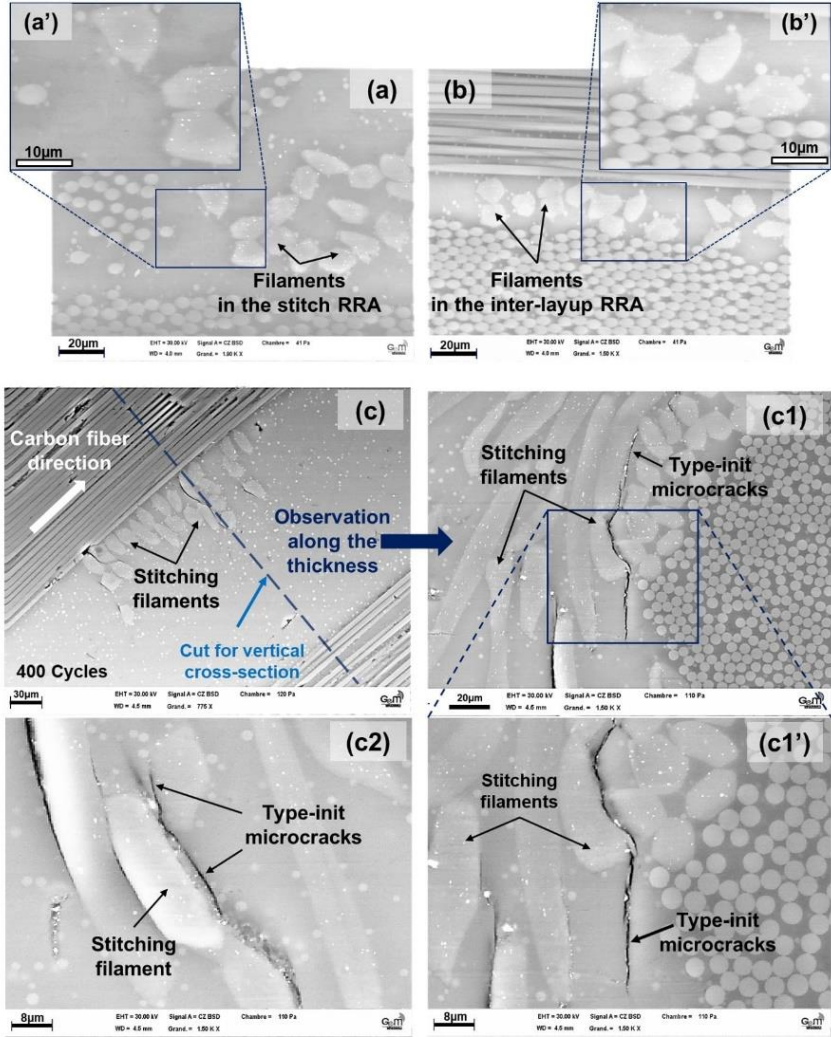


Figure 12. SEM observation of the unaged PET36-A sample in the stitch (a, a') and in the inter-layups (b, b'). Example of Type-init microcracks of the sample stitched with the PET 36 dtex yarn subjected to 400 cycles. SEM observation of the cross section on the surface (c) and along the thickness (c1, c1', c2).

Furthermore, the saturated PET36-A\_SAT sample was examined by scanning electron microscopy (SEM) after 800 hygrothermal cycles. The sample shows Type-init microcrack observed at the Resin/Stitching filament (or Epoxy/PET) interface (Figure 13-a', left), while decohesion appears to occur at the Resin/Stitching filament interface (Figure 13-a', right). Furthermore, Figure 13- (b, b') shows the presence of damage initiated at the

Resin/Carbon fiber interface. It seems that degradation phenomena due to physical and/or chemical aging occur in these interfaces during hygrothermal cycles. However, this remains a qualitative observation because it would be difficult to conclude without performing a physico-chemical characterization by appropriate instruments such as Differential Scanning Calorimetry (DSC), Dynamic Viscoelastometer, etc. Several authors show that moisture can cause degradation at the Resin/Carbon fiber interfaces which can reduce the resistance of the composites to microcracking [44,45]. This phenomenon requires a study of the physico-chemical characterization either at the “Resin/Stitching filament” or “Resin/Carbon fiber” interfaces in order to appropriately conclude on these complex degradation phenomena under hygrothermal aging. This physico-chemical characterization is unfortunately not carried out in this paper, but the SEM observations reveal great prospects and show the importance of its study for the understanding of the microcracking mechanism of the NCF composite subjected to hygrothermal cycles.

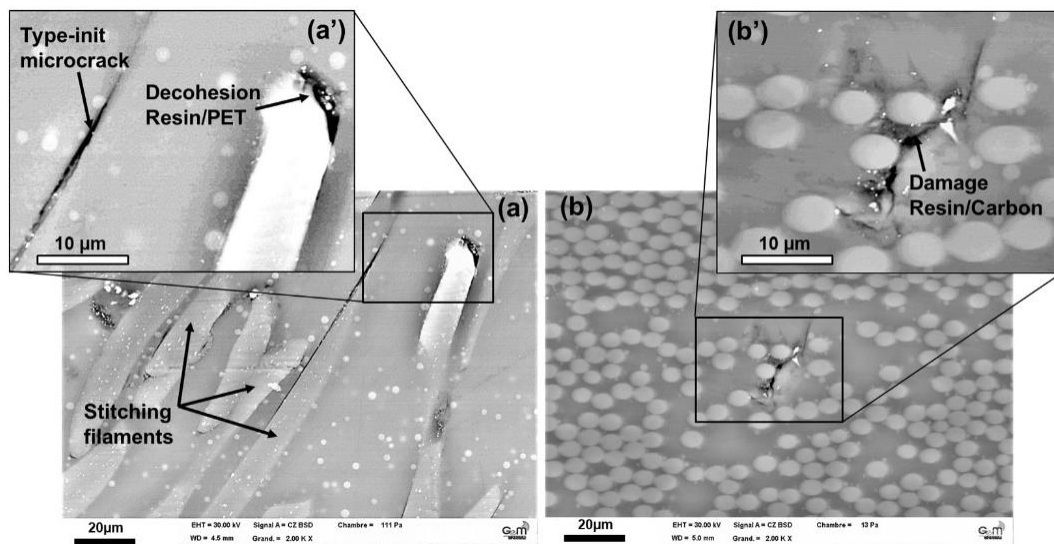


Figure 13. SEM observation of the initiation of microcracks at the carbon Fibers/Resin interface (a) and at the stitching Filament/Resin interface (b) on the PET36-A\_SAT sample after 800 cycles.

#### 5.4.2 Type-init microcrack propagation

The Figure 14 taken under the optical microscope, show some examples of the development and location of Type-init microcracks in PET36 laminates (Figure 14-a and b) and in PA39 laminates (Figure 14-c and d). It is useful to remind that the stitching filaments can be located either in the stitch RRA (Figure 6-a and Figure 12-a) or in the inter-layup RRA (Figure 6-b and Figure 12-b). According to all the microscopic observations made with the optical microscope and the SEM, some hypotheses can be put forward on the development of the type-init microcracks according to the hygrothermal cycles applied:

- It appears that after a number of hygrothermal cycles, the Type-init microcracks that would be formed in the previous cycles grow in length and propagate transversely along the NCF ply thickness. For example,

for sample PET36-A, the 1200 cycles generate Type-init microcracks of about 68  $\mu\text{m}$  in the fibrous zones (Figure 14-a) and about 85  $\mu\text{m}$  in the RRA. Then, these microcracks seem to develop during the last hydrothermal cycles so that they become transverse microcracks like the Type-2 microcrack of 2000 cycles as shown in Figure 14-b . Likewise, Type-init microcracks would have formed from the first cycles on the PA39-A sample, these reach a length of about 98  $\mu\text{m}$  at 1600 cycles (Figure 14-c) and cross the entire ply thickness (200  $\mu\text{m}$ ) at 2000 cycles to become either Type-1 microcracks if they propagate in the RRA stitches or Type-2 microcracks if they propagate in the fibrous areas as shown in (Figure 14-d).

- Furthermore, the microcracking results show that the evolution of the Type-init microcrack density is quite fast during the first hydrothermal cycles (Figure 9-a, **Erreur ! Source du renvoi introuvable.-a**). However, after 1200 cycles, the evolution of the Type-init microcrack densities progress slowly and tend to converge to a stable stage during the last cycles. This could be explained by the fact that some Type-init microcracks, formed by the first cycles, have developed and become Type-1 and/or Type-2 microcracks within the last cycles.

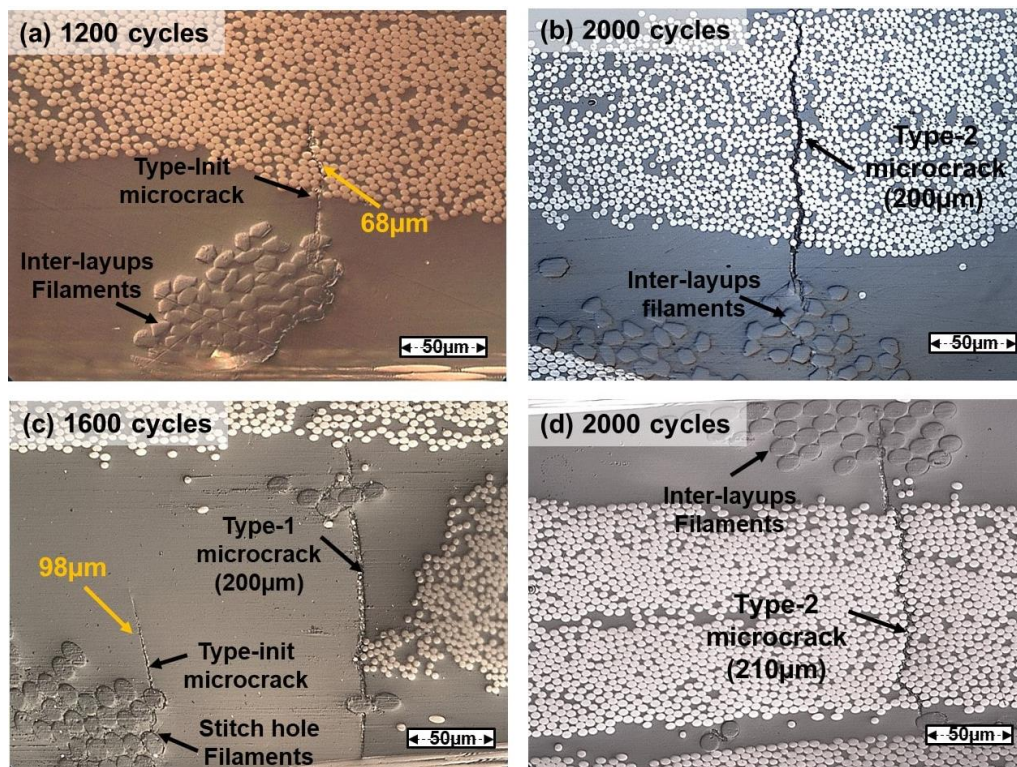


Figure 14. Example of each type of microcracks observed under an optical microscope after hydrothermal cycles. (a and b) PET36 NCF laminates. (c and d) PA39 NCF laminates.

The histogram shown in Figure 15 illustrates the development of the average length (in mm) of the Type init microcracks according to the hydrothermal cycles applied. It can be seen that for both samples PET36-B and

PA39-B, the average length of Type-init microcracks does not exceed 0.04 mm at 400 cycles, then it increases progressively with the applied cycles until reaching values lower than 0.12 mm.

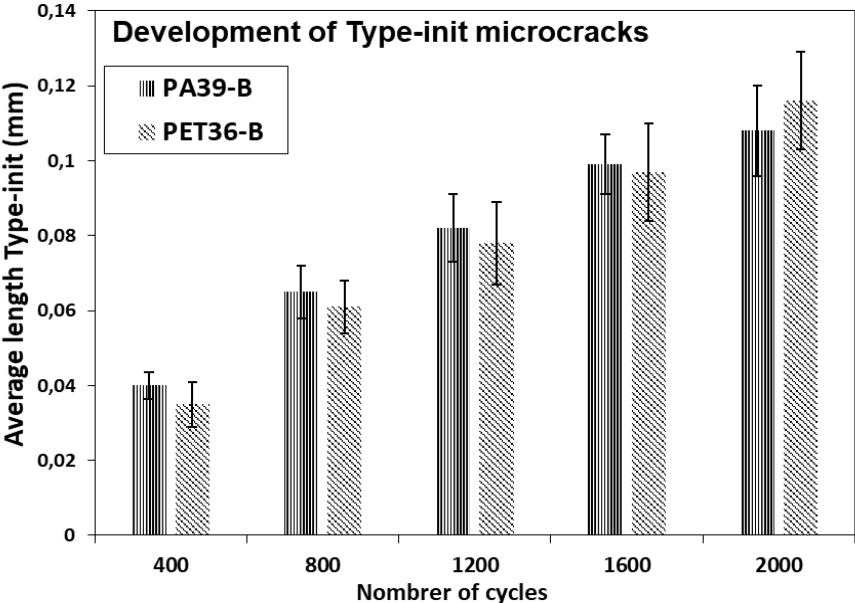


Figure 15. Development of the average length of Type-init microcracks with hygrothermal cycles.

**5.4.3 Propagation of transverse microcracks**

The in-plane 2D microscopic observations of the studied NCF samples show that the transverse microcracks detected in the RRA of the fisheye (Figure 16-a) propagate initially in the direction of the stitching yarn, which is generally oriented at 45° (Figure 16-c) with respect to the carbon fiber direction. These microcracks are damped by the fisheye edges (Fisheye RRA/Carbon fiber interfaces), as shown in Figure 16-b.

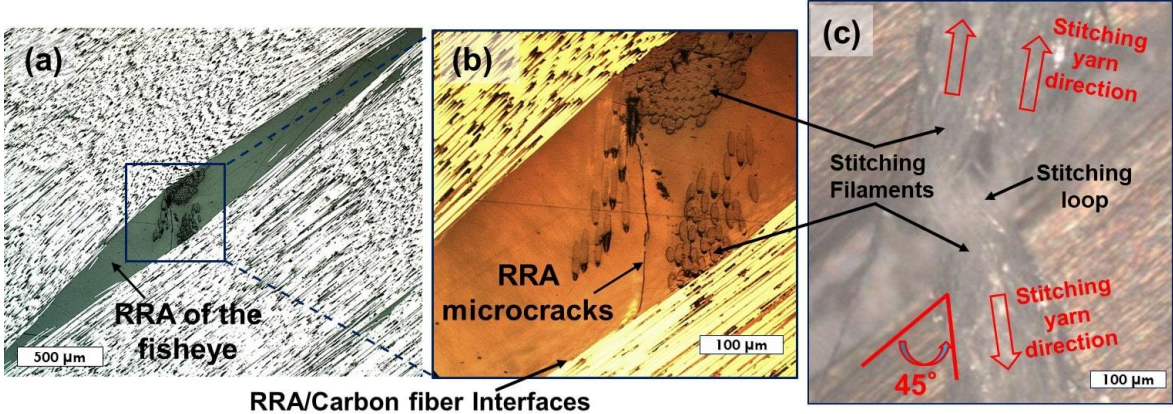


Figure 16. A PA39-B fisheye after 1200 hygrothermal cycles. The microcrack is oriented at 45° to the direction of the carbon fibers.

In order to obtain more information on the propagation and location of these microcracks, NCF samples were characterized by three-dimensional (3D) X-ray tomography. One of the main parameters for tomographic analysis of heterogeneous materials, such as NCF composites, is the contrast between the constituents, which are the matrix,

fibers, and stitching yarns. More technical details of X-ray tomography are explained in the review by Stock [46]. The microtomography system used is of reference XRadia XCT-400 (from École Centrale de Nantes) having a source between 40 kV and 150 kV. For the tests performed on a  $5 \times 5 \times 3 \text{ mm}^3$  PA39-B sample. The sample was cut to have at least one fisheye in each ply of the laminate. These dimensions are chosen as small as possible to obtain adequate resolution for 3D analyses. The applied voltage is 40 kV and the size of a selected pixel is about  $5 \mu\text{m}$  on one side. In order to extract the required information, it is first necessary to reconstruct the three-dimensional volume from a sequence of several hundred 2D images. However, the reconstructed volume sometimes presents a reduced resolution and a degraded contrast. Therefore, appropriate post-processing of the images (thresholding, filtering, etc.) and sometimes extensive segmentation will be required. Segmentation is the process of dividing, manually or automatically on the basis of their gray levels, the voxels of the 3D image into subgroups. However, automated segmentation on carbon NCF composites is a difficult technique, mainly due to the low difference between the contrasts of the Carbon/Resin/Stitching constituents. Figure 17 shows an example of detail separation (gray level) in the PA39-B laminate after removal of reinforcements (carbon fiber). Figure 17-a shows the distribution of resin-rich areas (in green, RRA in fisheyes and in inter-layups), Figure 17-b shows the polyamide stitching yarns (in blue), and Figure 17-c shows the transverse microcracks (in red).

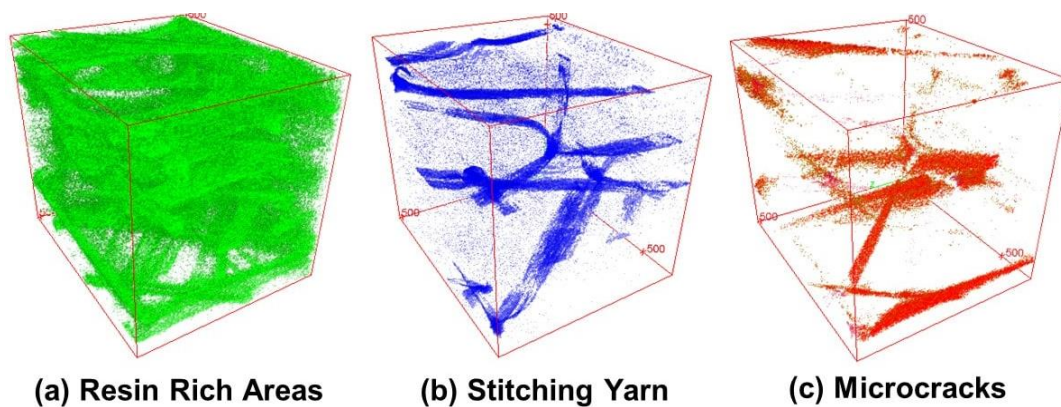


Figure 17. Highlighting of constituents and microcracks in NCF PA39-B subjected to 2000 hygrothermal cycles. Figure 18 shows the gray level projection of the PA39-B sample after the 3D volume reconstruction. This projection reveals Type-init microcracks at the Resin/Stitching filament interfaces (in red) and Type-1 microcracks in the RRA of the fisheyes. One of the main points of this figure is that Type-init microcracks are mostly located at the stitch loops (where the stitching yarn cross the NCF) and tend to follow filament lines: either on the surface at NCF inter-layups as shown in Figure 18-a and in the RRA of fisheye stitches as shown in Figure 18-(c, d, e).

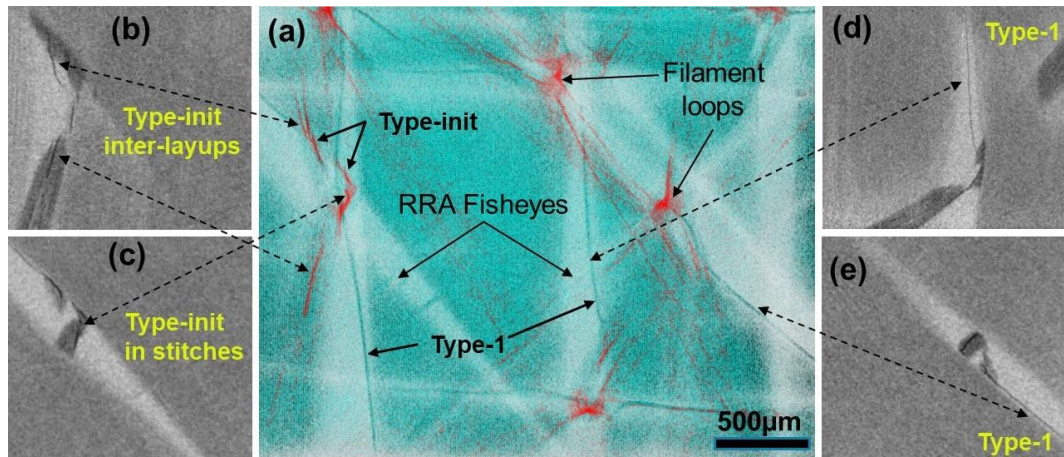


Figure 18. Projection of Type-init and Type-1 microcracks of PA39-B after 3D tomographic reconstruction.

Through qualitative observations of the reconstructed 3D volumes after 2000 accelerated hygrothermal cycles, we found that in each ply of the laminate, the transverse microcracks are all connected to the stitches and the orientation of a Type-1 microcrack corresponds to the orientation of the fisheye in which it propagates (Figure 19-a, b, c, f). Similarly, Type-2 microcrack is oriented along the direction of the carbon fibers (Figure 19-d, e). However, while the microcracks propagate well in the volume, it is difficult to know the exact length of the microcracks in this sample. It is necessary to observe a larger sample to obtain more information on the maximum length of the transverse microcracks in 3D volume. On the other hand, a very high resolution would be required to observe the Type-init microcracks in more precision at the interfaces of the stitching filaments.

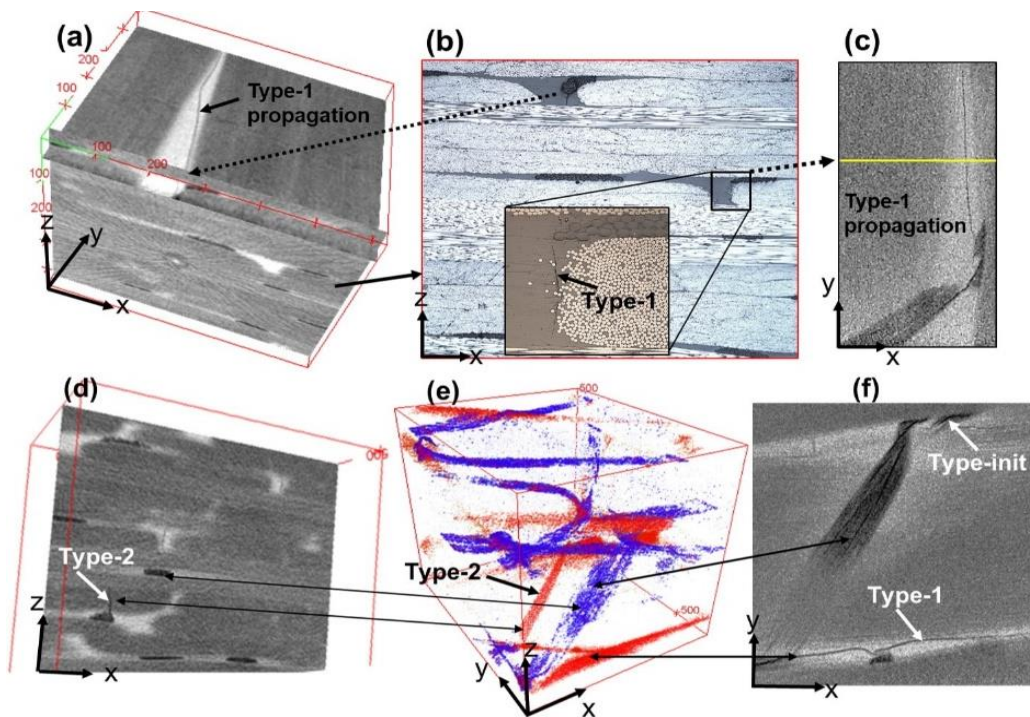


Figure 19. Propagation of microcracks in the volume of the PA39-B laminate.

## 6 Conclusion

In this study, an experimental approach to quantify microcracks under accelerated hygrothermal cycles of NCF laminates was presented. It was seen that the morphology of the NCF composite presents a multi-scale heterogeneity. The 2D method of characterizing specific microcracking allowed to study the evolution of microcracking during hygrothermal cycles by defining a microcrack density variable appropriate for NCF laminates. It was shown by 2D microscopic (Optical Microscope and SEM) and 3D tomographic X-ray observations that the local morphology of NCF composites is heterogeneous and the stitching yarn present at the different levels is at the origin of the RRA and the disturbance. In order to identify the origin of the microcracking, three types of microcracks are distinguished: Type-init are initiated at the stitching “Resin/Stitching filaments” interfaces, Type-1 appear in the RRA of the fisheyes (RRA of the NCF openings), Type-2 appear at the fibrous areas of the NCF, i.e. at the Resin/Carbon fibers areas. Type-init microcracks appear from the first cycles and their average length is between 40  $\mu\text{m}$  (at 400 cycles) and 120  $\mu\text{m}$  (at 2000 cycles). These microcracks can occur at several locations where the filaments are dispersed, either in the stitch RRA or in the inter-layup RRA. It was observed that Type-init microcracks are the first microcracks initiated in the studied samples and Type-2 microcracks generally appear after Type-1 microcracks. In addition, Type-init microcracks could propagate in the fisheye RRA to become Type-1 microcrack as they could propagate in carbon fiber areas to become Type-2 microcrack. Type-1 and Type-2 microcracks are transverse and cross the entire thickness of the ply. Due to the adapted microcrack density variable, comparisons could be made on these microcracks types.

Another comparison was carried out between laminates manufactured with two different options in order to identify the influence the biaxial NCF styles on the RRA and on the microcracking. The “option B” laminates (only one NCF style used, i.e. [+45/-45]) had less microcracks than the “option A” laminates (3 NCF styles used: [+45/-45], [-45/+45], [0/90]). The reason for this difference is that the RRA are more voluminous in biaxial NCF [0/90] styles. Indeed, it appears that the fisheye openings and lengths are larger in the 0 and 90 plies compared to the  $\pm 45$  plies, resulting in voluminous RRA in the NCF layups after laminate manufacturing. As a result, a higher RRA make the NCF composite more susceptible to microcracking in the hygrothermal cycle.

Finally, it was shown that moisture can have a beneficial role and thus limit microcrack densities in RRA. This can be explained by the relaxation of manufacturing and hygrothermal loading stresses in the matrix. However, this is not the case for microcracking at the “Resin/Carbon fibers” interfaces, since saturated samples have higher microcrack densities than unsaturated samples. Degradation at the “Epoxy/Carbon” interfaces due to moisture absorption may be the reason for this increase. This phenomenon is particularly complex as additional analyses must be performed in order to be able to identify the influence of moisture on the “Epoxy/Carbon” interfaces.

## Acknowledgments

This study was financed within the framework of the NCF-HP<sup>2</sup> project, involving 4 partners: Chomarat, Solvay, Mécanium and the University of Nantes. We would like to thank all the partners and funders of this project.

## References

- [1] Reynolds TG, McManus HL. Accelerated tests of environmental degradation in composite materials. *Compos. Struct. Theory Pract.*, ASTM International; 2001.
- [2] Henaff-Gardin C, Lafarie-Frenot MC, Gamby D. Doubly periodic matrix cracking in composite laminates part 1: General in-plane loading. *Compos Struct* 1996;36:113–130.
- [3] Gates T. 1 - The physical and chemical ageing of polymeric composites. In: Martin R, editor. *Ageing Compos.*, Woodhead Publishing; 2008, p. 3–33. <https://doi.org/10.1533/9781845694937.1.3>.
- [4] Shirrell CD, Halpin J. Moisture Absorption and Desorption in Epoxy Composite Laminates. *Compos Mater Test Des Fourth Conf* 1977.
- [5] Reifsnider KL, Dillard DA, Cardon AH. *PROGRESS IN DURABILITY ANALYSIS OF COMPOSITE SYSTEMS*. Virginia Polytechnic Institute and State University, USA; 1998.
- [6] Gigliotti M. Vieillissement, durabilité et dégradation de matériaux composites soumis à des environnements agressifs. *Sci Mater* 2012;37:299–313.
- [7] Jedidi J, Jacquemin F, Vautrin A. Accelerated hygrothermal cyclical tests for carbon/epoxy laminates. *Compos Part Appl Sci Manuf* 2006;37:636–645.
- [8] Maddocks JR. Microcracking in composite laminates under thermal and mechanical loading. Thesis. Massachusetts Inst. of Tech, 1996.
- [9] Park C, Mcmanus HL. Thermally induced damage in composite space structure: Predictive methodology and experimental correlation 1994;56:26.
- [10] Liotier PJ, Vautrin A, Beraud JM. Microcracking of composites reinforced by stitched multiaxials subjected to cyclical hygrothermal loadings. *Compos Part Appl Sci Manuf* 2011;42:425–437.
- [11] Mercier J. Prise en compte du vieillissement et de l'endommagement dans le dimensionnement de structures en matériaux composites. PhD Thesis. ENSAM, Paris, 2006.
- [12] S. V. Lomov. *Non-crimp fabric composites - Manufacturing, properties and applications*. Oxford Cambridge UK: Woodhead Publishing; 2011.
- [13] Renard J, Favre J-P, Jeggy Th. Influence of transverse cracking on ply behavior: Introduction of a characteristic damage variable. *Compos Sci Technol* 1993;46:29–37.
- [14] H. N. McManus. Prediction of thermal cycling induced cracking in polymer matrix composites 1993.
- [15] Hegde SR, Hojjati M. Effect of core and facesheet thickness on mechanical property of composite sandwich structures subjected to thermal fatigue. *Int J Fatigue* 2019;127:16–24.
- [16] Jacquemin F, Vautrin A. A closed-form solution for the internal stresses in thick composite cylinders induced by cyclical environmental conditions. *Compos Struct* 2002;58:1–9.
- [17] Meng M, Rizvi MJ, Grove SM, Le HR. Effects of hygrothermal stress on the failure of CFRP composites. *Compos Struct* 2015;133:1024–1035.
- [18] Vauthier E, Abry JC, Bailliez T, Chateauminois A. Interactions between hygrothermal ageing and fatigue damage in unidirectional glass/epoxy composites. *Compos Sci Technol* 1998;58:687–692.
- [19] Han M-H, Nairn JA. Hygrothermal aging of polyimide matrix composite laminates. *Compos Part Appl Sci Manuf* 2003;34:979–86.
- [20] Behera A, Vishwakarma A, Thawre MM, Ballal A. Effect of hygrothermal aging on static behavior of quasi-isotropic CFRP composite laminate. *Compos Commun* 2020;17:51–5.
- [21] Weitsman YJ. 2.11 - Effects of Fluids on Polymeric Composites—A Review. In: Kelly A, Zweben C, editors. *Compr. Compos. Mater.*, Oxford: Pergamon; 2000, p. 369–401. <https://doi.org/10.1016/B0-08-042993-9/00068-1>.
- [22] Mercier J, Bunsell A, Castaing P, Renard J. Characterisation and modelling of aging of composites. *Compos Part Appl Sci Manuf* 2008;39:428–38. <https://doi.org/10.1016/j.compositesa.2007.08.015>.
- [23] Smith L, Weitsman Y. The immersed fatigue response of polymer composites. *Int J Fract* 1996;82:31–42.
- [24] WEITSMAN Y. Chapter 9 - Moisture in Composites: Sorption and Damage. In: Reifsnider KL, editor. *Compos. Mater. Ser.*, vol. 4, Elsevier; 1991, p. 385–429. <https://doi.org/10.1016/B978-0-444-70507-5.50013-5>.

- [25] Morgan RJ, Shin EE, Drzal LT, Lee A. Characterization of critical fundamental aging mechanisms of high temperature polymer matrix composites. MICHIGAN STATE UNIV EAST LANSING COMPOSITE MATERIALS STRUCTURES CENTER; 1998.
- [26] Andreopoulos AG, Tarantili PA. Water sorption characteristics of epoxy resin–UHMPE fibers composites. *J Appl Polym Sci* 1998;70:747–55. [https://doi.org/10.1002/\(SICI\)1097-4628\(19981024\)70:4<747::AID-APP14>3.0.CO;2-U](https://doi.org/10.1002/(SICI)1097-4628(19981024)70:4<747::AID-APP14>3.0.CO;2-U).
- [27] Costa M, Almeida S, Rezende MC. Hygrothermal effects on dynamic mechanical analysis and fracture behavior of polymeric composites. *Mater Res-Ibero-Am J Mater - MATER RES-IBERO-AM J MATER* 2005;8. <https://doi.org/10.1590/S1516-14392005000300019>.
- [28] Truong TC, Ivanov DS, Klimshin DV, Lomov SV, Verpoest I. Carbon composites based on multi-axial multi-ply stitched preforms. Part 7: Mechanical properties and damage observations in composites with sheared reinforcement. *Compos Part Appl Sci Manuf* 2008;39:1380–1393.
- [29] Wei Y, Zhang J. Characterization of microstructure in stitched UD composite laminates. *Compos Part Appl Sci Manuf* 2008;39:815–824.
- [30] Vallons K, Adolphs G, Lucas P, Lomov SV, Verpoest I. The influence of the stitching pattern on the internal geometry, quasi-static and fatigue mechanical properties of glass fiber NCF composites. *Compos Part Appl Sci Manuf* 2014;56:272–279.
- [31] Meola C, Boccardi S, Carlomagno G maria. Chapter 1 - Composite Materials in the Aeronautical Industry. In: Meola C, Boccardi S, Carlomagno G maria, editors. *Infrared Thermogr. Eval. Aerosp. Compos. Mater.*, Woodhead Publishing; 2017, p. 1–24. <https://doi.org/10.1016/B978-1-78242-171-9.00001-2>.
- [32] Nguyen Thi Thuy Q. Identification des propriétés morphologiques et hygrothermiques hétérogènes de nouveaux composites hautes performances soumis à des cycles de vieillissement thermo-hygro-mécaniques. PhD Thesis. ENSM, 2013.
- [33] Liotier PJ, Alain V, Christine D. Characterization of 3D morphology and microcracks in composites reinforced by multi-axial multi-ply stitched preforms. *Compos Part Appl Sci Manuf* 2010;41:653–662.
- [34] Shipsha A, Burman M, Ekh J. Failure of cross-ply NCF composites under off-axis compressive loads - An experimental study and a new strength prediction model including fibre bundle waviness. *Compos Part B Eng* 2018;153:49–56.
- [35] Koissin V, Kustermans J, Lomov SV, Verpoest I, Van Den Broucke B, Witzel V. Structurally stitched NCF preforms: Quasi-static response. *Compos Sci Technol* 2009;69:2701–2710.
- [36] Mattsson D, Joffe R, Varna J. Methodology for characterization of internal structure parameters governing performance in NCF composites. *Compos Part B Eng* 2007;38:44–57.
- [37] Anand SC. Technical fabric structures – Knitted fabrics. In: Horrocks AR, Anand SC, editors. *Handb. Tech. Text.* 2nd Ed., Woodhead Publishing; 2016, p. 107–62. <https://doi.org/10.1016/B978-1-78242-458-1.00005-4>.
- [38] Klug, Jeremy Hager. High-performance adhesive systems for polymer composite bonding applications. PhD Thesis. University of Washington, 1999.
- [39] Youssef Z, Jacquemin F, Gloaguen D, Guillen R. A multi-scale analysis of composite structures: Application to the design of accelerated hygrothermal cycles. *Compos Struct* 2008;82:302–309.
- [40] Reynolds TG. Accelerated tests of environmental degradation in composite in materials. PhD Thesis. Department of Aeronautics, Massachusetts Institute of Technology, 1998.
- [41] Hottengada B. Investigation of Microcracking and Damage Propagation in Cross-Ply Composite Laminates. PhD Thesis Univ New Orleans 2006.
- [42] Zhong Y, Joshi SC. Impact behavior and damage characteristics of hygrothermally conditioned carbon epoxy composite laminates. *Mater Des* 2015;65:254–264.
- [43] Lomov SV, Belov EB, Bischoff T, Ghosh SB, Truong Chi T, Verpoest I. Carbon composites based on multi-axial multiply stitched preforms. Part 1. Geometry of the preform. *Compos Part Appl Sci Manuf* 2002;33:1171–83.
- [44] Costa ML, Almeida SFM de, Rezende MC. Hygrothermal effects on dynamic mechanical analysis and fracture behavior of polymeric composites. *Mater Res* 2005;8:335–340.
- [45] Niu Y-F, Yan Y, Yao J-W. Hygrothermal aging mechanism of carbon fiber/epoxy resin composites based on quantitative characterization of interface structure. *Polym Test* 2021;94:107019. <https://doi.org/10.1016/j.polymertesting.2020.107019>.
- [46] Stock SR. X-ray microtomography of materials. *Int Mater Rev* 1999;44:141–64. <https://doi.org/10.1179/095066099101528261>.